An Energy- and Enstrophy-Constrained Parameterization of Barotropic Eddy Potential Vorticity Fluxes

ROSIE E. EAVES,[a] JAMES R. MADDISON,[b] DAVID P. MARSHALL,[a] AND STEPHANIE WATERMAN[c]

[a] *Department of Physics, University of Oxford, Oxford, United Kingdom*
[b] *School of Mathematics and Maxwell Institute for Mathematical Sciences, The University of Edinburgh, Edinburgh, United Kingdom*
[c] *Department of Earth, Ocean and Atmospheric Sciences, The University of British Columbia, Vancouver, British Columbia, Canada*

(Manuscript received 14 February 2024, in final form 21 January 2025, accepted 5 February 2025)

ABSTRACT: A parameterization for barotropic eddy potential vorticity (PV) fluxes is introduced, which applies both an energetic and an enstrophetic constraint to a downgradient PV mixing closure. An eddy kinetic energy budget and an eddy potential enstrophy budget are employed to constrain the parameterized eddy PV fluxes. Through the budgets, the parameterization facilitates a bidirectional exchange of kinetic energy between the parameterized eddies and the large-scale flow and a conversion of potential enstrophy from the large-scale flow to the parameterized eddies. The parameterization is tested in simulations of barotropic, freely decaying turbulence in a doubly periodic domain over variable bottom topography. The simulations show that employing the parameterization results in an upscale transfer of kinetic energy on average, consistent with quasigeostrophic theory. Furthermore, the kinetic energy and potential enstrophy budgets employed are sufficient to constrain the large-scale flow in a realistic manner when compared to an eddy-resolving model. As a result, a topography-following flow of the correct magnitude emerges in a coarse-resolution model with parameterized eddy effects. Dissipation in the coarse-resolution simulations is significant, leading to the most significant source of discrepancy between the coarse-resolution simulation with parameterized eddy effects and the eddy-resolving simulation. This work constitutes a first step toward the ultimate aim of parameterizing both baroclinic and barotropic turbulence. How this may be achieved by integrating this parameterization with other methods in more realistic ocean simulations is discussed.

SIGNIFICANCE STATEMENT: Mesoscale eddies in the ocean, the analog of atmospheric weather systems, are an important factor in determining the large-scale flow. In particular, in regions where the height of the ocean floor varies, eddies drive the flow toward a structure which resembles that of the ocean floor. Commonly employed methods of representing eddies in climate models are unable to capture this process because they fail to represent accurately the underlying physical processes that constrain the eddies. Here, we present a method for representing ocean eddies in climate models, which uses the conservation of energy, and of a similar quantity that measures the amount of turbulent stirring, to constrain the feedback of the eddies on the large-scale flow. We test the new method experimentally in a simple computational ocean model, analyzing both the parameters that are important in the underlying physics and the properties of the large-scale flows produced by the eddies.

KEYWORDS: Eddies; Mesoscale processes; Parameterization

1. Introduction

Mesoscale eddies are a ubiquitous feature of the ocean and are known to affect the large-scale flow through a number of processes. The majority of CMIP6-class models with an ocean component are run at a spatial resolution which is unable to explicitly resolve the full mesoscale eddy field (Griffies et al. 2009; Eyring et al. 2016; Gregory et al. 2016; Griffies et al. 2016; Jones et al. 2016), and eddy parameterizations must be employed. One eddy-driven process which is typically neglected in eddy parameterizations commonly employed in CMIP6-class models is the interaction of the eddies with the seafloor, specifically in producing rectified topography-following flows. This study aims to develop a parameterization for barotropic mesoscale ocean eddies which can produce such flows by replicating the net effect of the cascades of energy and enstrophy associated with the barotropic mode.

Relevant to this parameterization development is the theory of quasigeostrophic turbulence (e.g., Salmon 1998). Briefly, energy and potential enstrophy are input to the ocean on large scales in the baroclinic modes. Quasigeostrophic theory predicts that these quantities cascade to smaller scales until, at scales close to the Rossby radius of deformation, the process of barotropization occurs. In this process, a portion of the available potential energy (APE) and kinetic energy in the baroclinic modes are converted to kinetic energy in the barotropic mode. Similarly, a portion of the potential enstrophy in the baroclinic modes is converted to potential enstrophy in the barotropic mode. In the barotropic mode, kinetic energy cascades to large scales where it is dissipated by bottom friction, and potential enstrophy cascades to small scales where it is dissipated by viscous effects.

The prevailing eddy parameterization in CMIP6-class models is Gent and McWilliams (1990) (hereafter referred to as

Denotes content that is immediately available upon publication as open access.

Corresponding author: Rosie Eaves, rosie.eaves@physics.ox.ac.uk

DOI: 10.1175/JPO-D-24-0027.1

GM90). GM90 parameterizes the eddy-induced transport arising from eddy buoyancy fluxes as a prescribed advection of tracers, resulting in an adiabatic flattening of isopycnals. A key feature of GM90, and one its successes, is ensuring the conservation of fluid volume between isopycnals. Through GM90, energy is extracted from APE in the large-scale[1] flow, thus mimicking one of the effects of baroclinic instability in the energy cascades described above. Quasigeostrophic theory predicts that some of the APE extracted by baroclinic eddies will be converted to barotropic eddy kinetic energy (EKE) and subsequently cascaded to large scales. However, GM90 does not attempt to parameterize the barotropic mode and this process remains unaccounted for in simulations employing GM90. Thus, GM90 introduces a sink of energy into the system, and without further parameterization methods, the effect of the barotropic mode of turbulence is neglected.

More recent work in the design of eddy parameterizations has incorporated additional conservation properties based on the fundamental law of energy conservation, leading to the development of energetically constrained parameterizations via the integration of a subgrid energy budget. The subgrid energy is then used to inform the eddy parameterization employed, for example, with variants of GM90 (e.g., Cessi 2008; Eden and Greatbatch 2008; Mak et al. 2017, 2018) or a downgradient potential vorticity (PV) mixing parameterization (Marshall and Adcroft 2010). Incorporating an energetic constraint has been shown to improve the energetics of the large-scale flow (Marshall and Adcroft 2010), as well as produce emergent features, such as eddy saturation in idealized models of the Southern Ocean circulation, consistent with the dynamics of eddy-resolving simulations (Mak et al. 2017, 2018).

Some eddy parameterization formulations also incorporate mechanisms to parameterize specific energy pathways. For example, it is a known problem that explicit diffusion, required in numerical models for stability, extracts energy at the grid scale (Jansen and Held 2014). Additionally, as described above, the extraction of APE from the large-scale flow by GM90 represents a loss of energy in the system (Bachman 2019). Backscatter has been proposed as a method of compensating for these artificial energy sinks in eddy-permitting models and involves accounting for the lost energy and reinjecting it to the resolved flow, typically via a negative Laplacian of the resolved velocity in the governing equation (Jansen and Held 2014; Jansen et al. 2015; Bachman 2019; Jansen et al. 2019; Juricke et al. 2019, 2020; Yankovsky et al. 2024). This re-energizes the resolved eddies, which can subsequently cascade the reinjected kinetic energy to larger scales. Incorporating a mechanism of backscatter has been shown to improve the kinetic energy spectra of the large-scale flow when compared to eddy-resolving simulations (Jansen and Held 2014; Jansen et al. 2015; Bachman 2019; Juricke et al. 2019; Yankovsky et al. 2024).

Jansen et al. (2019) extended the mechanism described above for use in noneddying as well as eddy-permitting models by combining a backscatter mechanism with an energetically constrained implementation of GM90. In this parameterization formulation, APE extracted from the system by GM90 can energize the resolved flow or energize the parameterized eddies through the energetically informed value of κ_{GM}. Yankovsky et al. (2024) added a vertical structure to the backscatter mechanism of Jansen et al. (2019), given by the equivalent barotropic mode, which produced more realistic energetics in eddy-permitting simulations than the combination of depth-independent backscatter with GM90 tested by Jansen et al. (2019).

Alternatively, parameterizing eddies in noneddying models using a downgradient PV mixing parameterization permits bidirectional conversion of kinetic energy between the large-scale flow and the eddies (Marshall and Adcroft 2010), with the direction of the energy transfer linked to Arnold's first stability theorem (Arnold 1965). In practice, this can lead to the forcing of large-scale flows that are consistent with the inverse cascade of KE, demonstrated, for example, in Waterman and Jayne (2012) and Tamarin et al. (2016).

While there are many instances in the literature of eddy parameterization formulations designed to respect energy dynamics, the same focus has not been applied as thoroughly to the dynamics of enstrophy. Quasigeostrophic theory predicts a direct cascade of potential enstrophy, which is dissipated at small scales. Potential enstrophy dissipation is guaranteed by design in downgradient PV closures and is ensured in some backscatter parameterizations by reinjecting the energy at scales larger than those at which it is extracted (Jansen and Held 2014; Jansen et al. 2015; Bachman 2019). However, to our knowledge, no parameterizations exist that explicitly consider a dynamical potential enstrophy budget and use this to constrain the parameterization.

Energy and enstrophy dynamics play a crucial role in the development of eddy-driven topography-following flows. Bretherton and Haidvogel (1976) hypothesized that the turbulent cascades of kinetic energy and potential enstrophy in barotropic turbulence drive the flow toward a minimum enstrophy state for a given initial energy, resulting in an eddy-driven topography-following flow. Recent evidence suggests that this hypothesis holds qualitatively true for low-energy states, in which the initial domain-integrated energy is less than that of a PV-homogenized state, but does not hold for high-energy states due to the emergence of coherent vortices (Siegelman and Young 2023; Gallet 2024). Numerical experiments have demonstrated that both the initial energy (Adcock and Marshall 2000; Siegelman and Young 2023) and initial enstrophy (Gallet 2024; He and Wang 2024) are important in determining the state of barotropic freely decaying turbulence over topography.

The importance of energy and enstrophy dynamics in eddy-driven topography-following flows is further evidenced by the inability of energetically unconstrained parameterizations (i.e., formulations in which there is no feedback of the subgrid energetics on the parameterized eddy effects) to produce realistic eddy-driven topography-following flows. For example, GM90 with constant eddy buoyancy diffusivity introduces a sink of energy over topography, resulting in an unrealistic

[1] In the context of eddy parameterizations, the terms large-scale and eddy are used to signify the resolved and unresolved dynamics, respectively.

state of rest, while downgradient PV mixing with a constant eddy PV diffusivity can introduce a spurious source of energy into the system (Adcock and Marshall 2000). In contrast, incorporating a backscatter mechanism in eddy-permitting models, thus reinvigorating the inverse kinetic energy cascade, can enhance topography-following flows (Jansen et al. 2015).

The hypothesis that eddies drive the flow toward a state of minimum enstrophy (Bretherton and Haidvogel 1976) can also be understood as eddies driving the flow toward a state of maximum entropy (Gallet 2024), which leads to topography-following flows. Holloway (1992) exploited this idea to develop the Neptune parameterization by using the cascades of energy and enstrophy inherent to the flow to derive a solution for the flow field with maximized entropy. The Neptune parameterization relaxes the resolved flow toward a simplified estimate of this maximum entropy flow field, which follows topographic contours resulting in an eddy-driven topography-following flow. However, Neptune does not respect energy conservation and, for this reason, implementation of Neptune in climate models is rare.

In this study, we present a parameterization of the eddy-mean flow interaction resulting from the barotropic eddy PV fluxes, with the aim of producing realistic emergent eddy-driven topography-following flows in noneddying models. The parameterization is formulated by incorporating physically motivated constraints into a downgradient PV mixing parameterization. We build on the success of previous energetically constrained parameterizations by implementing an energy constraint as well as an additional enstrophy constraint, implemented in a method analogous to that employed in energetically constrained parameterizations. The resulting parameterization

- employs a subgrid EKE budget and a subgrid eddy potential enstrophy (EPEnstr) budget to constrain the parameterized eddy PV fluxes;
- includes a mechanism through which kinetic energy can be exchanged bidirectionally between the unresolved eddies and the large-scale flow; and
- includes a mechanism through which potential enstrophy can be converted from the large-scale flow to the unresolved eddies.

We do not attempt to parameterize the effects of the baroclinic modes of turbulence within this parameterization. The ultimate aim is to produce a parameterization of barotropic eddies which can be implemented alongside, and integrated with, a parameterization of baroclinic turbulence. The integration of these parameterizations would mimic the process of barotropization, thus providing a source of parameterized barotropic eddies. Other mechanisms through which barotropic eddies are generated may also be incorporated in future work. As an initial proof of concept, we restrict our attention to barotropic turbulence, noting that satisfactory results of barotropic experiments are a prerequisite to testing in a baroclinic setup.

We test the functionality of the parameterization in noneddying simulations of barotropic, freely decaying turbulence in a doubly periodic domain over variable bottom topography on an f plane. We demonstrate that the parameterization results in a conversion of kinetic energy from the parameterized eddies to the large-scale flow on average, as well as a conversion of potential enstrophy from the large-scale flow to the parameterized eddies, consistent with the net effect of the cascades predicted by quasigeostrophic theory. Furthermore, we show that the energetic and enstrophetic constraints imposed in the parameterization are successful in constraining the large-scale, eddy-driven, topography-following flow such that it has realistic energy and enstrophy relative to the flow in an eddy-resolving simulation. Finally, we examine the sensitivity of the large-scale flow to the input parameters of the parameterization.

The rest of this article is structured as follows. In section 2, we outline the formulation of the proposed energetically and enstrophetically constrained downgradient PV mixing parameterization. In section 3, we describe our methods related to testing this parameterization in an idealized model, including the experimental design and details about the numerical model setup. In section 4, we compare the energetics and enstrophetics of a barotropic spin-down experiment with variable bottom topography at eddy-resolving resolution with the results of a coarse-resolution simulation in which no parameterization is employed in order to highlight what is required of the parameterization for this problem. We also diagnose the parameterization parameters from the eddy-resolving simulation for use in the parameterized simulation. In section 5, we present the results of parameterized simulations. In section 6, we discuss the work presented, and in section 7, we provide a summary.

2. An energetically and enstrophetically constrained downgradient PV mixing parameterization

This section outlines the method of incorporating an energetic and enstrophetic constraint into a downgradient PV mixing parameterization.

a. Downgradient PV mixing parameterizations

For a barotropic fluid, the PV, q, is defined as

$$q = \frac{f + \xi}{H}, \tag{1}$$

where f is the planetary vorticity; ξ is the vertical component of relative vorticity, defined as $\xi = \partial v/\partial x - \partial u/\partial y$, where u and v are the zonal (x) and meridional (y) components of the horizontal velocity $\mathbf{u}$ respectively; and H is the layer thickness.[2] We begin by performing a Reynolds average of the PV and the horizontal velocity to obtain

$$q = \overline{q} + q', \tag{2}$$

$$\mathbf{u} = \overline{\mathbf{u}} + \mathbf{u}', \tag{3}$$

where the overbars denote a time mean, used to represent the large-scale, slowly evolving component of the flow, which we refer to as the mean field; and the primes denote a deviation from this time mean, used to represent the small-scale, fast-evolving

[2] Note that H must be invariant with time in order for Eq. (4) to be true. In the experiments discussed and analyzed in this paper, we consider one vertical layer with a rigid lid and a bottom topography that is invariant with time. Hence, this requirement is satisfied.

component of the flow, which we refer to as the eddy field. Downgradient PV mixing parameterizations parameterize the eddy PV fluxes as the mixing of PV down the mean PV gradient at a specified rate controlled by an eddy diffusivity. This takes the form

$$\overline{q'\mathbf{u}'} = -\kappa_{\mathrm{PV}}\nabla\overline{q}, \tag{4}$$

where κ_{PV} is the eddy PV diffusivity.

An unconstrained PV mixing parameterization, i.e., a downgradient PV mixing parameterization in which κ_{PV} is a constant in time and space, will continue to act on a flow until there are no PV gradients. That is, it will always drive the flow toward PV homogenization. However, Siegelman and Young (2023) demonstrate that for freely decaying, two-dimensional turbulence over topography, numerical simulations with an initial energy below that of a PV-homogenized state do not reach a state of PV homogenization. This can be understood from an energy conservation perspective: If the initial energy is below that of a PV-homogenized state, an energy input would be required to reach PV homogenization. Thus, by indiscriminately driving the flow to a PV-homogenized state, an unconstrained PV mixing parameterization can introduce a spurious source of energy into the system. We will demonstrate this phenomenon in section 5. We aim to eliminate this spurious source of energy such that the large-scale flow resembles that of an eddy-resolving simulation by implementing physically motivated constraints on the value of κ_{PV}.

b. Constraining the eddy PV diffusivity

To constrain the time-mean eddy PV fluxes, $\overline{q'\mathbf{u}'}$, we exploit the following bound:

$$|\overline{q'\mathbf{u}'}|^2 \le \overline{|q'|^2}\;\overline{|\mathbf{u}'|^2} = 4\Lambda K, \tag{5}$$

where Λ is the EPEnstr and K is the EKE, defined as

$$\Lambda = \frac{\overline{q'^2}}{2}, \tag{6}$$

and

$$K = \frac{\overline{u'^2} + \overline{v'^2}}{2}, \tag{7}$$

respectively, and where we have used the Cauchy–Schwarz inequality in Eq. (5). This bound holds, for example, for eddy-mean decomposition via time averaging as used in this study.

We now employ a similar approach to Marshall et al. (2012) to construct a downgradient PV mixing parameterization from Eq. (5). A dimensionless efficiency parameter, γ_q, can be defined from the bound in Eq. (5), such that

$$|\overline{q'\mathbf{u}'}| = 2\gamma_q\sqrt{\Lambda K}, \tag{8}$$

where $0 \le \gamma_q \le 1$. When $\gamma_q = 0$, the eddy PV flux is zero on average. In this case, the eddies do not have a net effect on the large-scale flow. When $\gamma_q = 1$, the eddy PV flux magnitude is at its maximum value and the effect of the eddies on the large-scale flow is maximized. Hence, γ_q describes how efficient the eddies are at fluxing PV and we refer to it as the PV flux efficiency parameter.

Equation (5) leads to the following downgradient PV mixing parameterization:

$$\overline{q'\mathbf{u}'} = -2\gamma_q\sqrt{\Lambda K}\;\widehat{\nabla\overline{q}}, \tag{9}$$

where $\widehat{\ }$ denotes a unit vector. Note that Eq. (9) satisfies the bound in Eq. (5) due to the constraint on the magnitude of γ_q.

Equation (9) describes a downgradient PV mixing parameterization in which the eddy PV diffusivity is determined by the EKE, the EPEnstr, and the PV flux efficiency parameter which is bounded by unity. Hence, a key feature of the parameterization is that the magnitude of the eddy PV fluxes is determined by both the EKE and EPEnstr in the system. Physically, Eq. (9) implies that both EPEnstr, i.e., PV anomalies, and EKE, i.e., eddies, are required for an eddy PV flux to be present. In other words, if there are no eddies, or if the PV is uniform, there will be no eddy PV flux.

The choice to include a factor of -1 in Eq. (9) imposes downgradient PV mixing by design. One caveat to this approach is that, while it is true that the eddies flux PV down the mean PV gradient on average (Marshall and Adcroft 2010), this is not necessarily the case locally (e.g., Waterman and Jayne 2012). However, imposing downgradient PV mixing is a common tactic in eddy parameterization design (e.g., Treguier et al. 1997; Marshall and Adcroft 2010; Eden 2010), and we deem it an appropriate assumption for this first demonstration-of-concept exercise.

It should be noted that Eq. (9) does not satisfy the integral constraint necessary for the conservation of angular momentum in a zonal channel on a β plane (Marshall 1981; Marshall et al. 2012). Here, we test the functionality of the parameterization in a doubly periodic basin on an f plane in which this integral constraint is less of a concern. While extending the parameterization to satisfy this constraint for use in a zonal channel setup is out of the scope of this study, we discuss possible options based on the literature in section 6.

It remains to determine Λ and K for use in informing the parameterization. One strategy for determining these parameters used widely in the literature (e.g., Eden and Greatbatch 2008; Cessi 2008; Marshall and Adcroft 2010; Marshall et al. 2012; Mak et al. 2017, 2018; Jansen et al. 2019; Yankovsky et al. 2024) is to employ prognostic equations, i.e., budgets, for unresolved, subgrid-scale quantities. We adopt this strategy here, stepping forward budgets for the depth-averaged values of Λ and K at each time step and using the time-evolving values of Λ and K to inform the parameterization. The intention of this formulation is that the parameterization's dependence on time-evolving budgets of Λ and K will act to realistically constrain the energy and enstrophy of the resolved flow.

c. The eddy kinetic energy budget

The depth-integrated EKE equation is

$$H\frac{\partial}{\partial t}\left(\frac{\overline{\mathbf{u}'\cdot\mathbf{u}'}}{2}\right) = H\overline{q'\mathbf{u}'}\cdot\nabla\overline{\psi} - \nabla\cdot H\overline{\mathbf{u}'B'} + \mathbf{F}_{\mathrm{EKE}}, \tag{10}$$

where ψ is the transport streamfunction; B is the Bernoulli potential defined as $B = \mathbf{u}\cdot\mathbf{u}/2 + p/\rho_0$, where p is the pressure and ρ_0 is the reference density; and $\mathbf{F}_{\mathrm{EKE}}$ represents the sources and sinks of EKE.

We construct a parameterized EKE budget from Eq. (10). The first term on the right-hand side of Eq. (10) represents the kinetic energy conversion between the large-scale flow and the eddies, discussed in more detail below. The second term on the right-hand side integrates to zero over the domain and therefore acts only to redistribute the energy. Following the literature (e.g., Eden and Greatbatch 2008; Marshall and Adcroft 2010; Jansen et al. 2019; Yankovsky et al. 2024), we represent this redistribution of depth-integrated EKE as advection by the large-scale flow and Laplacian diffusion with coefficient μ. Finally, we include only a sink of EKE through bottom friction in $\mathbf{F}_{\mathrm{EKE}}$, which we parameterize as linear drag with coefficient r_K. Thus, our depth-averaged parameterized EKE budget is

$$\frac{\partial K}{\partial t} = \overline{q'\mathbf{u}'} \cdot \nabla\overline{\psi} - \frac{1}{H}\nabla \cdot (KH\overline{\mathbf{u}}) + \frac{\mu}{H}\nabla^2 HK - r_K K, \qquad (11)$$

where K is now the subgrid-scale parameterized EKE, the overbars represent the resolved values (which represent the mean/large-scale components in parameterized simulations), and the eddy parameterization [Eq. (9)] is used to evaluate $\overline{q'\mathbf{u}'}$.

The first term on the right-hand side of Eq. (11) represents kinetic energy conversion between the large-scale flow and the parameterized eddies (Marshall and Adcroft 2010) with a positive value signifying conversion from the large-scale flow to the eddies. This term also appears in the budget of Marshall and Adcroft (2010) where it is shown to represent a parameterized analog of Arnold's first stability theorem (Arnold 1965). This term is capable of converting kinetic energy from the parameterized eddies to the large-scale flow, mimicking the inverse cascade typical of quasigeostrophic turbulence; however, the magnitude and direction of the conversion will depend on the values of the parameterized EKE and EPEnstr due to the formulation of the parameterized eddy PV fluxes [Eq. (9)]. This term differs from the energy backscatter term in, for example, Jansen and Held (2014), Jansen et al. (2015), Bachman (2019), Jansen et al. (2019), Yankovsky et al. (2024) in several ways: 1) It represents a distinct energy pathway; i.e., it represents the conversion of kinetic energy between the large-scale flow and the eddies as opposed to the compensation of extracted energy; 2) it allows for bidirectional kinetic energy conversion, i.e., the parameterized eddies can accelerate the large-scale flow, and/or the large-scale flow can accelerate the parameterized eddies (Marshall and Adcroft 2010); 3) it is analytically derived as opposed to inserted in the budget as a forcing term; and 4) it does not require the use of a negative Laplacian in the governing equation to re-energize the large-scale flow, which leads to a backscattering of energy whenever and wherever there is a resolved flow.

d. The eddy potential enstrophy budget

The depth-integrated EPEnstr equation is

$$H\frac{\partial}{\partial t}\left(\frac{\overline{q'^2}}{2}\right) = -H\overline{q'\mathbf{u}'} \cdot \nabla\overline{q} - \nabla \cdot \left(\frac{\overline{q'^2}}{2}H\overline{\mathbf{u}}\right) - \nabla \cdot \left(H\frac{\overline{q'^2}}{2}\mathbf{u}'\right) + \mathbf{F}_{\mathrm{EPEnstr}}, \qquad (12)$$

where $\mathbf{F}_{\mathrm{EPEnstr}}$ represents the sources and sinks of EPEnstr.

We construct a parameterized EPEnstr budget from Eq. (12). The first term on the right-hand side of Eq. (12) represents the conversion of potential enstrophy between the large-scale flow and the eddies, discussed in more detail below. The second and third terms represent the advection of depth-integrated EPEnstr by the large-scale and eddy components of the flow, respectively. We neglect the third term since it is a product of three eddy terms (Marshall and Shutts 1981), although numerical simulations indicate that this term is important in the redistribution of EPEnstr (Wilson and Williams 2004). We include both the damping of depth-integrated EPEnstr and viscous diffusion in $\mathbf{F}_{\mathrm{EPEnstr}}$, which we represent as linear and Laplacian damping with coefficients r_Λ and μ, respectively. Thus, our depth-averaged parameterized EPEnstr budget is

$$\frac{\partial \Lambda}{\partial t} = -\overline{q'\mathbf{u}'} \cdot \nabla\overline{q} - \frac{1}{H}\nabla \cdot (\Lambda H\overline{\mathbf{u}}) + \frac{\mu}{H}\nabla^2 H\Lambda - r_\Lambda \Lambda, \qquad (13)$$

where Λ is now the subgrid-scale parameterized EPEnstr, overbars represent the resolved values (which represent the mean/large-scale components in parameterized simulations), and the eddy parameterization [Eq. (9)] is used to evaluate $\overline{q'\mathbf{u}'}$.

Analogous to the first term on the right-hand side of the parameterized EKE budget, the first term on the right-hand side of Eq. (13) represents the potential enstrophy conversion between the large-scale flow and the parameterized eddies. Let us first consider this term in the context of Eq. (12), that is, in the EPEnstr budget of a fluid. When $-\overline{q'\mathbf{u}'} \cdot \nabla\overline{q}$ is positive, the eddy PV flux is, on average, down the mean PV gradient, that is, the eddies act to mix PV. This mixing of PV by the eddies results in a conversion of potential enstrophy from the large-scale component of the flow to the eddy component, i.e., a direct potential enstrophy cascade. When $-\overline{q'\mathbf{u}'} \cdot \nabla\overline{q}$ is negative, the eddy PV flux is, on average, up the mean PV gradient, i.e., the eddies act to unmix PV, resulting in a conversion of potential enstrophy from the eddy component to the large-scale component. Quasigeostrophic theory predicts that this term is positive on average, producing a direct cascade of potential enstrophy, but we note it may be positive locally (Holland and Rhines 1980). Now, let us consider this term in the context of the parameterized EPEnstr budget [Eq. (13)]. Due to the formulation of the parameterization, which imposes downgradient mixing of PV by construction [Eq. (9)], this term will always be positive in simulations that employ the parameterization to model the eddy effects. Thus, the parameterization acts only to mix PV and converts potential enstrophy from the large-scale flow to the parameterized eddy component only.

e. Parameterization summary

The energetically and enstrophetically constrained specification of downgradient eddy PV fluxes, the EKE budget, and the EPEnstr budget [Eqs. (9), (11), and (13), respectively] describe the parameterization fully. There are four input parameters to the parameterization: the PV flux efficiency parameter, γ_q; the EKE and EPEnstr diffusivity, μ; the EKE

TABLE 1. Parameters used in the simulations analyzed in sections 4 and 5. In the sensitivity experiments analyzed in section 5c, the parameter values of $50km_{EECON}$ are systematically varied by ±50% of the values stated for $50km_{EECON}$.

Configuration	Resolution (km)	Eddy parameterization	μ_ξ ($m^4\ s^{-1}$)	γ_q	r_Λ (s^{-1})	r_K (s^{-1})	μ ($m^{-2}\ s^{-1}$)	κ_{PV} ($m^2\ s^{-1}$)
$5km_{EXP}$	5	None	10^8	—	—	—	—	—
$50km_{NOPAR}$	50	None	10^{11}	—	—	—	—	—
$50km_{UNCON}$	50	Eq. (4)	10^{11}	—	—	—	—	60
$50km_{EECON}$	50	Section 2	10^{11}	0.1	5.0×10^{-8}	0	500	—

dissipation coefficient, r_K; and the EPEnstr dissipation coefficient, r_Λ. The initial distributions of parameterized EKE, K_0, and parameterized EPEnstr, Λ_0, must also be specified. The terms K and Λ evolve with time through the time integration of their respective budgets, and the time-evolving values are then used to determine the magnitude of the downgradient eddy PV fluxes at each time step. Through these budgets, the parameterization accounts for the bidirectional conversion of kinetic energy between the large-scale and eddy components, the dissipation of EKE, the conversion of potential enstrophy from the large-scale component to the eddy component through the mixing of PV, and EPEnstr dissipation.

3. Methods

a. Experimental design

To analyze the performance of the parameterization, we implement it in an idealized experimental setup, with which we aim to answer the following key questions:

1) Does the parameterization result in a net conversion of kinetic energy from the parameterized eddy field to the large-scale flow resulting in a topography-following flow?
2) Do the parameterized energetics and enstrophetics exhibit similar behavior to their explicit counterparts in an eddy-resolving simulation?
3) How do the input parameters to the parameterization affect the energetics and enstrophetics of the simulated flow?

To answer these questions, we run a set of numerical simulations in which we simulate barotropic, freely decaying turbulence over variable bottom topography on an f plane in a doubly periodic domain. The large-scale flow produced by this setup in an eddy-resolving simulation is an eddy-driven topography-following flow (section 4). We use the following four configurations:

(i) an eddy-resolving (5-km horizontal resolution) simulation with explicitly resolved eddies ($5km_{EXP}$);
(ii) a coarse-resolution (50-km horizontal resolution) simulation without employing any eddy parameterization ($50km_{NOPAR}$);
(iii) a coarse-resolution simulation with parameterized eddies where we employ an unconstrained downgradient PV mixing parameterization, i.e., Eq. (4) with constant eddy PV diffusivity, κ_{PV} ($50km_{UNCON}$);
(iv) a coarse-resolution simulation with parameterized eddies as described in section 2, i.e., with an energetically and enstrophetically constrained downgradient PV mixing parameterization ($50km_{EECON}$).

We choose to employ the parameterization in simulations with a horizontal resolution of 50 km as this corresponds to a noneddying resolution in much of the ocean where the Rossby radius of deformation is typically $O(10)$ km. For simulations which do not employ any eddy parameterization ($5km_{EXP}$ and $50km_{NOPAR}$), we perform a Reynolds average of the variables [as described in Eqs. (2) and (3)] to separate the flow into mean and eddy components, representing the large-scale slowly evolving component of the flow and the small-scale fast-evolving component of the flow, respectively. In $50km_{EECON}$, the "mean" and "eddy" components are defined as the resolved field and the unresolved parameterized field, respectively. The aim is that, in $50km_{EECON}$, the effect of the unresolved parameterized eddies on the resolved flow resembles the effect of the explicit eddies on the mean flow in the eddy-resolving simulation $5km_{EXP}$, thus leading to a resolved flow in $50km_{EECON}$, which resembles the mean flow in $5km_{EXP}$.

We compare $50km_{EECON}$ with $50km_{UNCON}$ to assess if the energetic and enstrophetic constraints imposed are successful in constraining the resolved flow. Note that EKE and EPEnstr budgets are not employed in $50km_{UNCON}$, and hence, these quantities are not well defined in this setup. We use $5km_{EXP}$ as a reference to inform on realistic values for the resolved flow, thus allowing us to determine if the resolved flow in the coarse-resolution simulation is well constrained by the parameterization. The details of these simulations are outlined in Table 1. We also run many variations of $50km_{EECON}$ varying the input parameters to the parameterization for each simulation in section 5c.

b. Model equations

We simulate freely decaying turbulence in a barotropic fluid (i.e., one vertical layer) with a rigid lid. The equations of motion are as follows: the depth-integrated PV equation, which, for simulations which do not employ any eddy parameterization, is

$$\frac{\partial \overline{\xi}}{\partial t} = -\nabla \cdot \overline{\zeta}\overline{\mathbf{u}} - \mu_\xi \nabla^4 \overline{\xi}, \tag{14}$$

and for parameterized eddy simulations is

$$\frac{\partial \overline{\xi}}{\partial t} = -\nabla \cdot \overline{\zeta}\overline{\mathbf{u}} - \nabla \cdot \overline{\zeta'\mathbf{u}'} - \mu_\xi \nabla^4 \overline{\xi}, \tag{15}$$

where the eddy PV flux term, $\nabla \cdot \overline{\zeta'\mathbf{u}'}$, is replaced with the appropriate parameterization, $\zeta = f + \xi$ is the absolute vorticity,

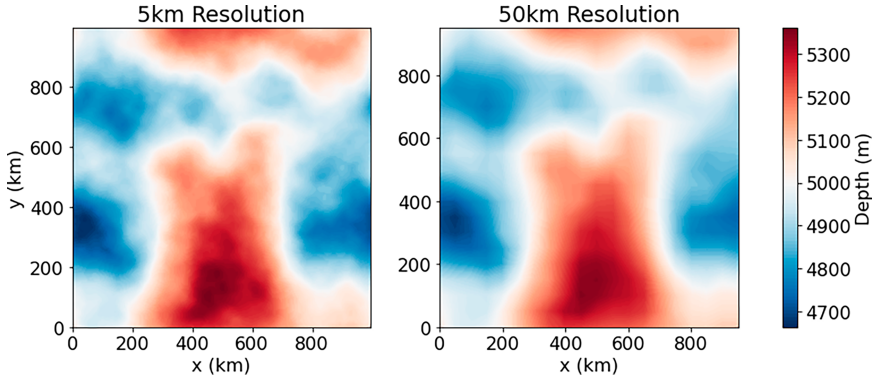

FIG. 1. Topography used in (left) high-resolution simulations and (right) coarse-resolution simulations.

and μ_ξ is the coefficient of biharmonic diffusion, employed for numerical stability; and the continuity equation,

$$\nabla \cdot H\overline{\mathbf{u}} = 0. \tag{16}$$

c. Numerical implementation

Time stepping of Eqs. (14) and (15) is performed as follows. The variables are arranged with vorticity, streamfunction, and layer depth defined at the cell vertices. The zonal and meridional components of the velocity are calculated using a centered second-order differencing scheme. Advection is calculated using an energy- and enstrophy-conserving scheme defined by Arakawa (1966). The biharmonic diffusion of vorticity is calculated using a centered differencing scheme. For parameterized simulations, K and Λ are defined at the cell center points. Time stepping of Eqs. (11), and (13)–(15) is computed using the third-order Adams–Bashforth method, with the first two time steps calculated using a first-order forward approximation. For $50\text{km}_{\text{EECON}}$, a minimum value for $|\nabla\overline{q}|$ is specified in the calculation of $\widehat{\nabla\overline{q}}$ to prevent division by zero, which we set at 10^{-16} m^{-1} s^{-1}. We set a minimum value of zero for K and Λ to ensure negative values of K and Λ are not generated.

d. Specification of domain geometry

All simulations are run in a periodic square domain of side length $L = 1000$ km with nonflat topography. The topography is created by using a seeded pseudorandom number generator to generate independent Fourier modes using a Gaussian distribution at 5-km resolution. A peak wavenumber of value 1 is specified when generating the Fourier modes. The field generated by the Fourier modes is then multiplied by a constant and translated in depth in order to produce a topography with an average depth of 5 km and depth variations of around 10%. The topography is regridded using spatial averaging to 50-km resolution for the coarse-resolution simulations. The topographic structures used are shown in Fig. 1.

e. Specification of model parameters

The Coriolis parameter is taken as a constant with value $f = 0.7 \times 10^{-4}$ s^{-1} in all simulations. The biharmonic diffusion coefficient, μ_ξ, is set to 10^8 m^4 s^{-1} for simulations at 5-km resolution and 10^{11} m^4 s^{-1} for simulations at 50-km resolution. These values are chosen to be as small as possible such that gridscale noise is no longer generated and give an eddy diffusive time scale on the order of months. All simulations are run for a total of 3000 days in order to reach a point at which the energy conversion from eddy to mean has plateaued. The value of parameters to be used in the parameterized simulations is diagnosed from the eddy-resolving simulation in section 4.

f. Specification of initial conditions

Simulations which do not employ any eddy parameterization (5km_{EXP} and $50\text{km}_{\text{NOPAR}}$) are initialized with a streamfunction which is generated at 5-km resolution using a similar method as that of the topography using a different seed. The peak wavenumber value specified for the initial streamfunction is 5. The field generated by the Fourier modes is multiplied by a constant to produce velocities on the order $O(1)$ cm s^{-1}. This streamfunction is regridded using volume averaging to 50-km resolution for use in $50\text{km}_{\text{NOPAR}}$. The initial streamfunctions are plotted in Fig. 2. In both 5km_{EXP} and $50\text{km}_{\text{NOPAR}}$, since there are no forcing terms, it is assumed that the eddies are driving the large-scale flow. This effect is expected to be small in $50\text{km}_{\text{NOPAR}}$ due to the coarse resolution, allowing for the identification of the missing physics when compared to 5km_{EXP}. Simulations with parameterized eddies ($50\text{km}_{\text{EECON}}$ and $50\text{km}_{\text{UNCON}}$) are run with no initial streamfunction, and instead, the parameterized eddies drive the flow.

The initial streamfunction employed here corresponds to a low-energy state in the classification defined in Siegelman and Young (2023), in which low-energy and high-energy states are defined as being below or above the energy of a PV-homogenized state, respectively. With the setup employed here, the maximum absolute value of the streamfunction for a PV-homogenized state is 575 Sv (1 Sv $\equiv 10^6$ m^3 s^{-1}). This is significantly stronger than the Antarctic Circumpolar Current, the world's strongest ocean current, which measurements estimate to be 173 Sv in the Drake Passage (Donohue et al. 2016). Thus, we deem high-energy states to be unnecessarily unrealistic for the

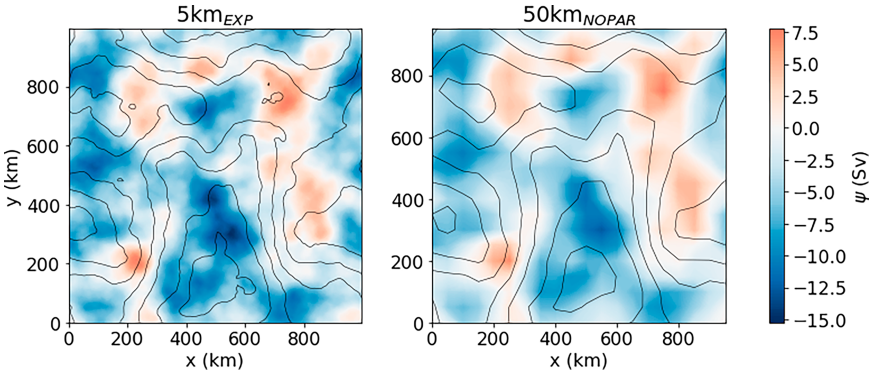

FIG. 2. Initial streamfunction used in simulations without any eddy parameterization at (left) 5-km resolution (namely, 5km$_{EXP}$) and (right) 50-km resolution (namely, 50km$_{NOPAR}$). Black contours indicate the topography.

testing purposes presented here and restrict our attention to low-energy states.

4. Explicit eddy simulations

a. *Identifying the unresolved eddy effects*

We compare the properties of the large-scale and eddy components of the flow in the eddy-resolving and coarse-resolution simulations, 5km$_{EXP}$ and 50km$_{NOPAR}$, respectively, to identify the unresolved eddy-driven effects on the large-scale flow in the coarse-resolution simulation. Throughout the rest of this paper, for simulations which do not employ any eddy parameterization (i.e., 5km$_{EXP}$ and 50km$_{NOPAR}$), the time-mean kinetic energy (MKE), defined as $|\overline{\mathbf{u}}|^2/2$, is used to represent the large-scale/mean component of the flow; the EKE is defined as $\overline{\mathbf{u}'\cdot\mathbf{u}'}/2$; the time-mean potential enstrophy (MPEnstr), defined as $|\overline{q}|^2/2$, is used to represent the large-scale/mean component of the potential enstrophy; and the EPEnstr is defined as $\overline{q'q'}/2$. Volume-averaged quantities are analyzed, and moving-window time means are taken every 50 days over a 500-day period.

We first identify the effects of the eddies on the energetics which are unresolved in the coarse-resolution simulation and hence need to be parameterized. In 5km$_{EXP}$, kinetic energy is converted from eddy to mean as the simulation progresses, indicated by the simultaneous decrease in EKE and increase in MKE (Figs. 3a,b). In contrast, for 50km$_{NOPAR}$, the EKE decreases throughout the simulation, but the MKE does not increase; hence, there is no significant conversion of kinetic energy from eddy to mean; the decrease in EKE in this case is due to damping from the biharmonic dissipation term. This is further illustrated by the eddy-to-mean kinetic energy conversion rate, which is large and positive throughout the majority of the simulation in 5km$_{EXP}$ and near-zero throughout the majority of the simulation in 50km$_{NOPAR}$ (Fig. 3c). Hence, we aim to parameterize the effects of this unresolved conversion on the large-scale flow, i.e., to parameterize a source of large-scale kinetic energy that mimics the effects of the eddy-to-mean kinetic energy conversion present in the eddy-resolving configuration.

We next identify the effects of the eddies on the enstrophetics, which are unresolved in the coarse-resolution simulation and, hence, need to be parameterized. In 5km$_{EXP}$, the mean-to-eddy potential enstrophy conversion term is positive throughout the simulation, meaning that the eddy PV fluxes are, on average, fluxing PV down the mean PV gradient, thus producing a conversion of potential enstrophy from mean to eddy and a direct potential enstrophy cascade (Fig. 3f). As a result, the MPEnstr decays for the duration of the simulation, shown by a negative change in MPEnstr (Fig. 3d). The EPEnstr also decays throughout the simulation due to dissipation of potential enstrophy at small scales (Fig. 3e). In 50km$_{NOPAR}$, both the potential enstrophy conversion term and the EPEnstr are small in comparison to 5km$_{EXP}$ (Figs. 3e,f). Additionally, the change in MPEnstr is positive, indicating an increase in MPEsntr (Fig. 3d). This increase in MPEnstr comes from the biharmonic diffusion term, which acts to bring the flow toward a state of rest, leading to a convergence of MPEnstr to that of the topographic PV (f/H). Thus, we require the parameterization to increase the potential enstrophy conversion term, to act to decrease the MPEnstr and increase the EPEnstr.

b. *Diagnosing the input parameters for the parameterized simulations*

Having identified the effect of the unresolved eddies which must be parameterized, we now seek to determine the appropriate values for the input parameters of the parameterization, namely, γ_q, the PV flux efficiency parameter; r_Λ, the EPEnstr damping parameter; r_K, the EKE damping parameter; and μ, the EKE and EPEnstr diffusion coefficient. We must also specify K_0 and Λ_0, the initial values for parameterized EKE and EPEnstr, respectively.

Figure 4a shows a scatter of the magnitude of the eddy PV fluxes $|\overline{q'\mathbf{u}'}|$, against their upper bound value $2\sqrt{\Lambda K}$ for all grid points in 5km$_{EXP}$, showing that the bound in Eq. (5) is indeed satisfied by all points in the domain. The line of best fit for the points, the gradient of which represents the average value of γ_q, has value 0.17 (blue line). Although there is some spatial structure in γ_q in 5km$_{EXP}$ (not shown), as a first attempt, we specify a constant value for γ_q, which we set to 0.1.

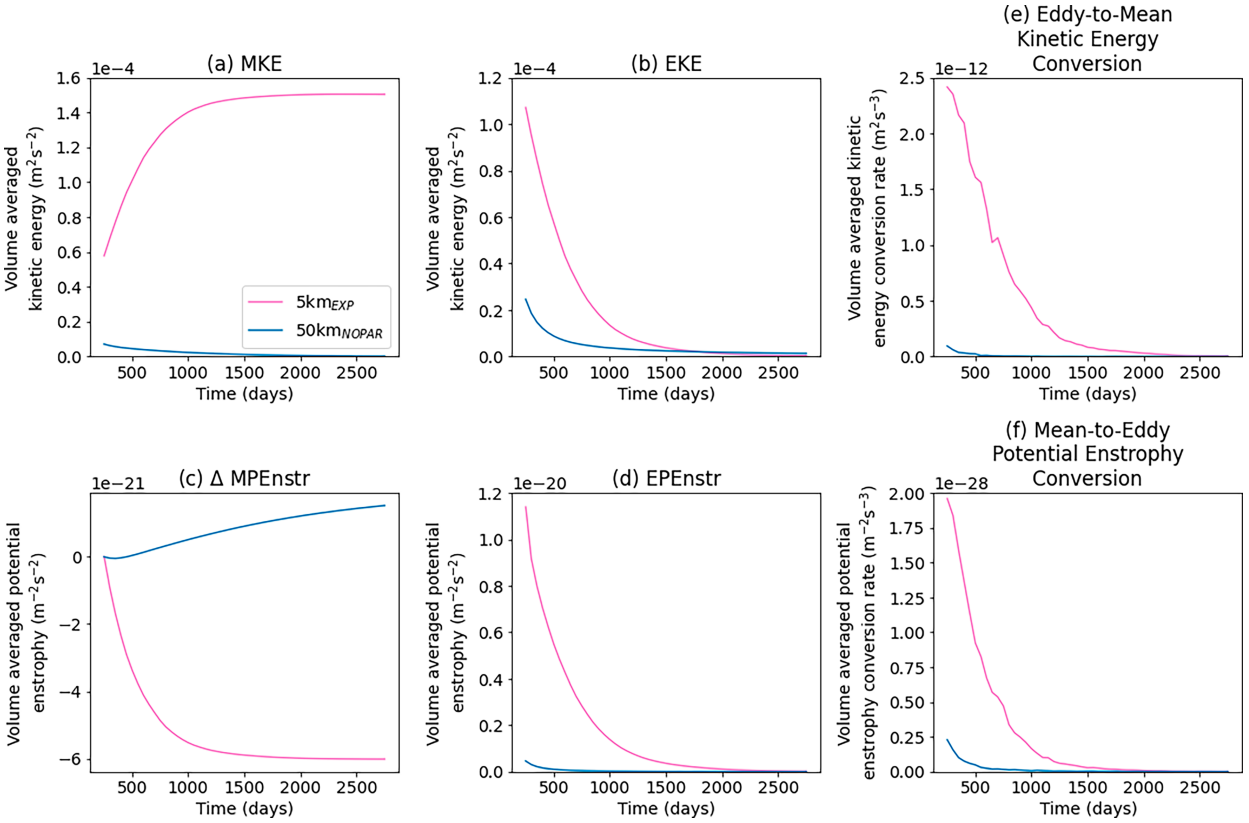

FIG. 3. Volume-averaged (a) MKE; (b) EKE; (c) eddy-to-mean kinetic energy conversion, $-\overline{q'\mathbf{u}'}\cdot\nabla\overline{\psi}$; (d) change in MPEnstr from the initial value; (e) EPEnstr; and (f) mean-to-eddy potential enstrophy conversion, $-\overline{q'\mathbf{u}'}\cdot\nabla\overline{q}$, for 5km_{EXP} (pink) and $50\text{km}_{\text{NOPAR}}$ (blue). Moving-window time means are calculated every 50 days over a 500-day period.

In a weakly dissipative regime, typical of freely decaying turbulence, energy is largely conserved while potential enstrophy is dissipated. To mimic these conditions, we set $r_K = 0\ \text{s}^{-1}$, i.e., we do not exert a damping effect on the parameterized EKE, and employ a nonzero value for r_Λ, which dissipates parameterized EPEnstr. We diagnose r_Λ from 5km_{EXP} by assuming that EPEnstr behaves as linear damping, taking the volume integral of the EPEnstr equation [i.e., the area integral of Eq. (12) with $\mathbf{F}_{\text{EPEnstr}} = -r_\Lambda(\overline{q'^2}/2)$] and integrating in time. The results are plotted in Fig. 4b showing that r_Λ varies in time with an initially larger value, which decays as the simulation progresses. For simplicity in our setup, we choose to use a constant value for r_Λ, which we set as the average value of those plotted in Fig. 4b, i.e., $5.0 \times 10^8\ \text{s}^{-1}$.

We set the EKE and EPEnstr diffusivity, μ, in Eqs. (11) and (13) to $500\ \text{m}^2\ \text{s}^{-1}$ to give a diffusive time scale on the order of months, consistent with that of the biharmonic diffusion term in the governing equation [Eqs. (14) and (15)].

The initial distributions of K and Λ must also be specified. For simplicity, we use constant values K_0 and Λ_0, respectively. We specify K_0 such that the volume-integrated initial parameterized EKE in $50\text{km}_{\text{EECON}}$ is the same as the volume-integrated initial kinetic energy of 5km_{EXP}, resulting in $K_0 = 1.8 \times 10^{-4}\ \text{m}^2\ \text{s}^{-2}$. The term Λ_0 is set to a similar value to the first time-mean volume-averaged value of Λ in 5km_{EXP}, resulting in $\Lambda_0 = 10^{-20}\ \text{m}^{-2}\ \text{s}^{-2}$.

For the coarse-resolution simulation with unconstrained eddy PV fluxes $50\text{km}_{\text{UNCON}}$, a constant value of κ_{PV} must be specified. We set this to the average of the nonzero values of κ_{PV} in simulation $50\text{km}_{\text{EECON}}$, which is $60\ \text{m}^2\ \text{s}^{-1}$.

5. Results of parameterized simulations

We now analyze the results of the parameterized simulations, focusing on the three key questions outlined in section 3. For parameterized simulations, i.e., $50\text{km}_{\text{EECON}}$ and $50\text{km}_{\text{UNCON}}$, the MKE is defined as the instantaneous resolved kinetic energy, i.e., $|\mathbf{u}|^2/2$; and the MPEnstr is defined as the instantaneous resolved potential enstrophy, i.e., $|q|^2/2$. For $50\text{km}_{\text{EECON}}$, the EKE and EPEnstr are the parameterized values, i.e., K and Λ, respectively. We compare the instantaneous values in the parameterized simulations with the time-mean values in the eddy-resolving simulation since we want to determine how well the parameterization simulates the large-scale flow.

a. *Topography-following flow*

The parameterization produces a net eddy-to-mean kinetic energy conversion, shown by the simultaneous decrease in parameterized EKE (Fig. 5b) and increase in MKE (Fig. 5a) in

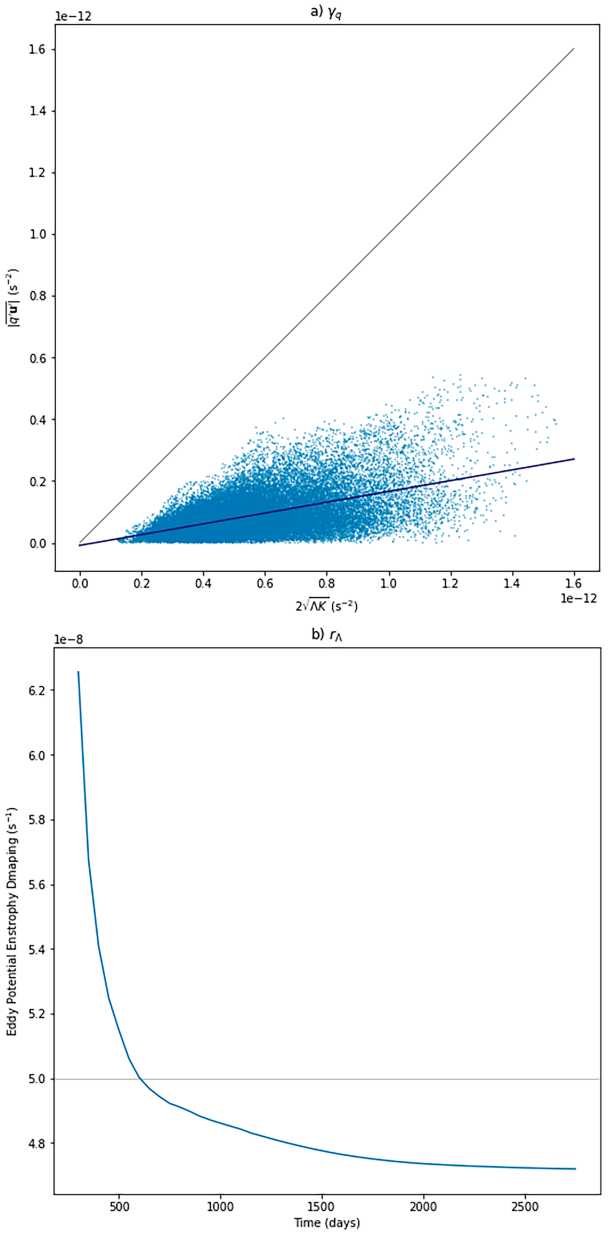

FIG. 4. (a) Scatterplot of the magnitude of the time-mean eddy PV fluxes, $|\overline{q'\mathbf{u}'}|$, against their upper bound value, $2\sqrt{\Lambda K}$, for all grid points in 5km$_{\mathrm{EXP}}$. The black line indicates the values where $|\overline{q'\mathbf{u}'}| = 2\sqrt{\Lambda K}$, and hence, the region to the right of the black line indicates the values where $|\overline{q'\mathbf{u}'}| \leq 2\sqrt{\Lambda K}$. The blue line indicates the line of best for the points and has slope 0.17. Means are taken over the entire 3000-day simulation period, and each point represents a grid point in the simulation. (b) The EPEnstr damping parameter, r_Λ, for 5km$_{\mathrm{EXP}}$. This is calculated from the EPEsntr equation [Eq. (13)] where time means are taken every 50 days over a 500-day period. The horizontal line indicates the parameterized EPEnstr linear damping coefficient r_Λ used in the simulation 50km$_{\mathrm{EECON}}$.

50km$_{\mathrm{EECON}}$. This is further confirmed by the parameterized kinetic energy conversion in 50km$_{\mathrm{EECON}}$, which is positive throughout the simulation (Fig. 5c). As a result of this parameterized eddy-to-mean kinetic energy conversion, a large-scale topography-following flow is produced (Fig. 6). The transition to a topography-following flow is also evidenced by the time evolution of the relationship between the streamfunction, ψ, and the PV, q (Fig. 7),[3] which evolves to a state in which the streamfunction becomes a function of PV in both 5km$_{\mathrm{EXP}}$ and 50km$_{\mathrm{EECON}}$. The relationship between ψ and q in 5km$_{\mathrm{EXP}}$ is well replicated by 50km$_{\mathrm{EECON}}$ at 900 days but deviates from that of 5km$_{\mathrm{EXP}}$ at 1800 days due to the stronger biharmonic diffusion, which dominates the forcing of the flow at this time in 50km$_{\mathrm{EECON}}$.

b. *Energetics and enstrophetics*

We now consider the effects of the parameterization on the energetics and enstrophetics. The peak magnitude of volume-averaged MKE is 1.5×10^{-4} m^2 s^{-2} in both 5km$_{\mathrm{EXP}}$ and 50km$_{\mathrm{EECON}}$. In contrast, the MKE in 50km$_{\mathrm{UNCON}}$ increases throughout the simulation, reaching a peak magnitude of 9.9×10^{-3} m^2 s^{-2}, over 60 times greater than the maximum MKE of 5km$_{\mathrm{EXP}}$. This suggests that the kinetic energy of the resolved flow is indeed well constrained by the energetic and enstrophetic constraints imposed in the parameterization. This is further illustrated by the magnitude of the transport streamfunction, which peaks at a value of 24.9, 18.9, and 202.2 Sv in 5km$_{\mathrm{EXP}}$ (Fig. 6), 50km$_{\mathrm{EECON}}$ (Fig. 6), and 50km$_{\mathrm{UNCON}}$ (Fig. 8), respectively. Thus, the peak magnitude of the transport streamfunction in 50km$_{\mathrm{UNCON}}$ is over 700% larger than that of 5km$_{\mathrm{EXP}}$, while in 50km$_{\mathrm{EECON}}$, it is 76% of that of 5km$_{\mathrm{EXP}}$.

The behavior of the MPEnstr is also improved by introducing the energetic and enstrophetic constraints. The mean-to-eddy potential enstrophy conversion in 50km$_{\mathrm{EECON}}$ is positive and nonzero initially, resulting in a decrease in the MPEnstr and an increase in the EPEnstr as required (Figs. 5d–f). The maximum absolute change in volume-averaged MPEnstr for 5km$_{\mathrm{EXP}}$, 50km$_{\mathrm{EECON}}$, and 50km$_{\mathrm{UNCON}}$ is 6.0×10^{-21}, 1.2×10^{-20}, and 6.7×10^{-20} m^{-2} s^{-2}, respectively. Thus, the maximum absolute change in MPEnstr in 50km$_{\mathrm{UNCON}}$ is more than 11 times that of 5km$_{\mathrm{EXP}}$, while the maximum absolute change in MPEnstr of 50km$_{\mathrm{EECON}}$ is twice that of 5km$_{\mathrm{EXP}}$. Physically, the MPEnstr in 50km$_{\mathrm{EECON}}$ decreases initially as the eddies mix PV (resulting in a positive mean-to-eddy potential enstrophy conversion) and increases when the parameterized eddies stop mixing PV and the biharmonic dissipation term dominates. In contrast, the MPEnstr in 50km$_{\mathrm{UNCON}}$ decreases throughout the simulation as PV continues to be mixed. This difference can be seen in the final PV for each simulation (Fig. 9). The 5km$_{\mathrm{EXP}}$ and 50km$_{\mathrm{EECON}}$ simulations exhibit similar final PV magnitudes, whereas the PV in 50km$_{\mathrm{UNCON}}$ is more mixed and therefore closer to PV homogenization. For clarity, we also include the PV of 50km$_{\mathrm{EECON}}$ at 265 days, when the MPEnstr is at a minimum and hence the time at which PV homogenization is maximized, which is also comparable in magnitude to that of 5km$_{\mathrm{EXP}}$.

[3] The PV plotted is that of Eq. (1), leading to a nonzero intercept in the q–ψ linear fit in Fig. 7. When the quasigeostrophic PV is used, the linear fit would pass through the origin.

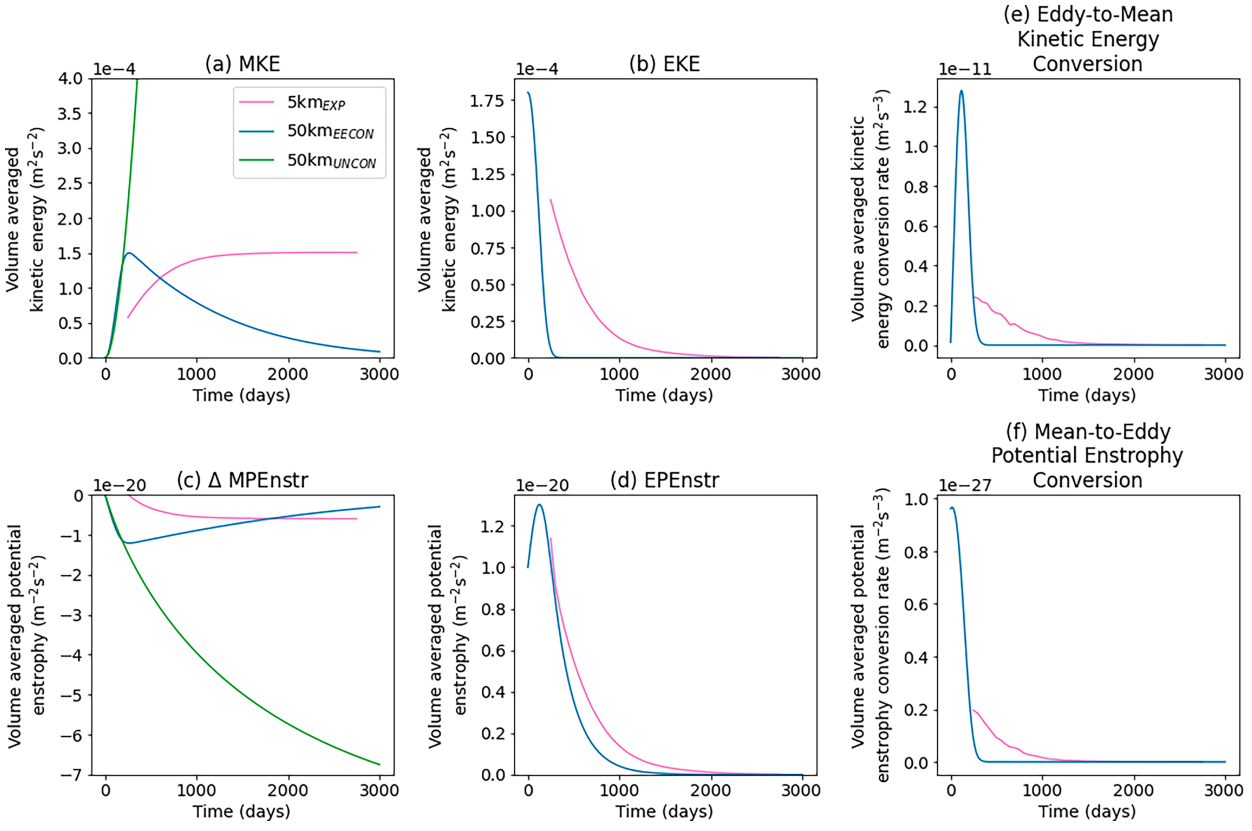

FIG. 5. Volume-averaged (a) MKE; (b) EKE; (c) eddy-to-mean kinetic energy conversion $-\overline{q'u'}\cdot\nabla\overline{\psi}$; (d) change in MPEnstr from the initial value; (e) EPEnstr; and (f) mean-to-eddy potential enstrophy conversion, $-\overline{q'u'}\cdot\nabla\overline{q}$, for 5km$_{EXP}$ (pink), 50km$_{EECON}$ (blue), and 50km$_{UNCON}$ (green). For 5km$_{EXP}$, the values shown are moving-window time means calculated every 50 days over a 500-day period. For 50km$_{EECON}$ and 50km$_{UNCON}$, the values shown are the instantaneous values. Note that data for 50km$_{UNCON}$ are not plotted in (b), (c), (e), and (f) since EKE and EPEnstr budgets are not employed in this simulation.

Both the eddy-to-mean kinetic energy conversion and mean-to-eddy potential enstrophy conversion in 50km$_{EECON}$ are of the correct order of magnitude but are initially larger than their counterparts in 5km$_{EXP}$ (Figs. 5c,f). This causes the MKE and MPEnstr to initially grow and decay, respectively, at a faster rate in 50km$_{EECON}$ than in 5km$_{EXP}$ (Figs. 5a,d). It is possible that the input parameters to the parameterization affect the time scale for the growth of MKE, and therefore, that tuning of the parameters could lead to a growth rate of MKE in 50km$_{EECON}$ that is more similar to that of 5km$_{EXP}$. However, here we focus on the functionality of the parameterization and do not seek to find optimally tuned parameters. We investigate the effect of varying the input parameters on the resolved flow in the following section.

One clear difference between 5km$_{EXP}$ and 50km$_{EECON}$ is that 5km$_{EXP}$ reaches a quasi-steady state, whereas 50km$_{EECON}$ returns to a state of no flow. Analysis shows that the damping of MKE and increase in MPEnstr in 50km$_{EECON}$ come from biharmonic diffusion (not shown). It is a known problem that explicit diffusion in models, required for numerical stability, dampens energy at the grid scale (Jansen and Held 2014). Since the biharmonic diffusion coefficient is larger in 50km$_{EECON}$ than in 5km$_{EXP}$, more kinetic energy is damped at the grid scale by explicit diffusion in 50km$_{EECON}$ than in 5km$_{EXP}$. This acts to bring the system back toward a state of no flow, leading to an increase in the MPEnstr.

c. *Sensitivity to input parameters*

We now test the sensitivity of the parameterization performance to the input parameters (γ_q, r_Λ, and μ) and the initial conditions (K_0 and Λ_0) by running a set of simulations in which we systematically vary these parameters. We compare the total amount of eddy-to-mean kinetic energy conversion throughout the simulation, the total amount of mean-to-eddy potential enstrophy conversion throughout the simulation, and the time taken for 90% of the initial parameterized EKE to be depleted as these parameters vary. Since the growth of MKE is due to the eddy-to-mean kinetic energy conversion, we use the time scale for depletion of parameterized EKE as a proxy for the time scale of the growth of MKE.

The total (time-integrated) volume-averaged eddy-to-mean kinetic energy conversion (Fig. 10) is predominantly determined by the initial amount of parameterized EKE, K_0, shown by the large variations in Figs. 10a–d compared with the relatively small variations in Figs. 10e–j. Figures 10e–j show a slightly larger total amount of kinetic energy converted

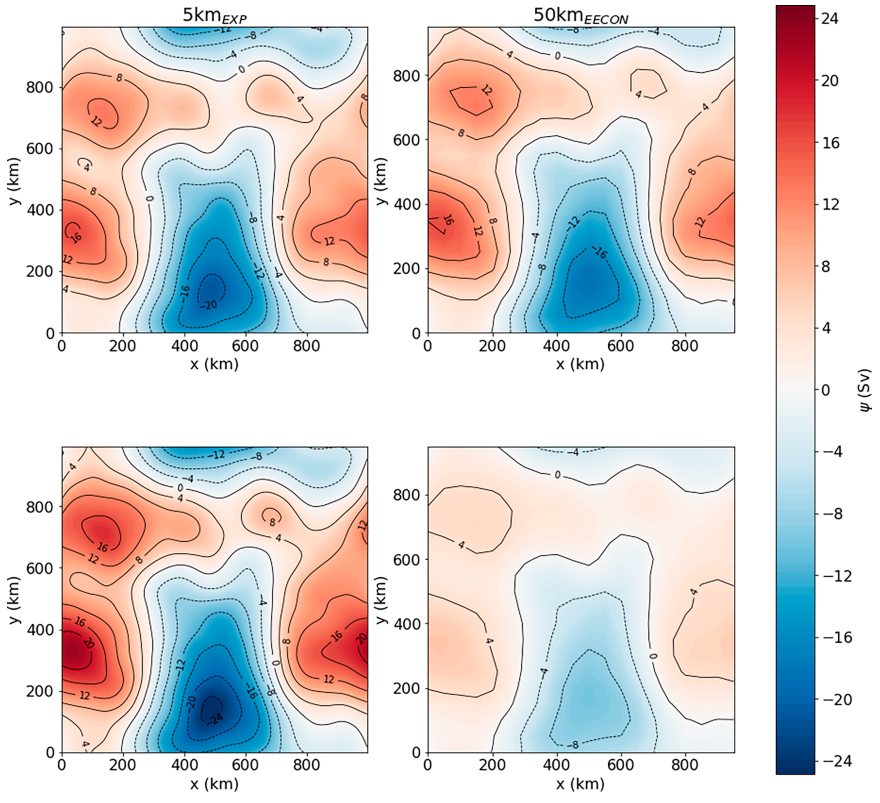

FIG. 6. Time-mean transport streamfunction for $5km_{EXP}$ (left) and $50km_{EECON}$ (right) over the time periods: (top) 0–1500 days and (bottom) 1501–3000 days.

than is available in the initial state (1.8×10^{-4} m^2 s^{-2}), which likely comes from numerical effects. However, the flow is still well constrained in these simulations determined by the maximum MKE compared to that of $5km_{EXP}$ (not shown).

The total (time-integrated) volume-averaged mean-to-eddy potential enstrophy conversion (Fig. 11) is also predominantly determined by K_0. This aligns with the result of Adcock and Marshall (2000) that eddies mix PV (i.e., convert potential enstrophy from mean to eddy) by an amount set by the energy of the initial state. The total amount of potential enstrophy converted is largely unaffected by μ and, rather counterintuitively, increases with increasing r_Λ and decreasing γ_q. This can be explained by the variation in time scale for the growth of MKE, or, more precisely, the time scale for the depletion of EKE (Fig. 12). This time scale increases with decreasing γ_q. A decrease in γ_q decreases the magnitude of the eddy PV fluxes through Eq. (9). This decrease in fluxes decreases the magnitude of the kinetic energy conversion term in the EKE

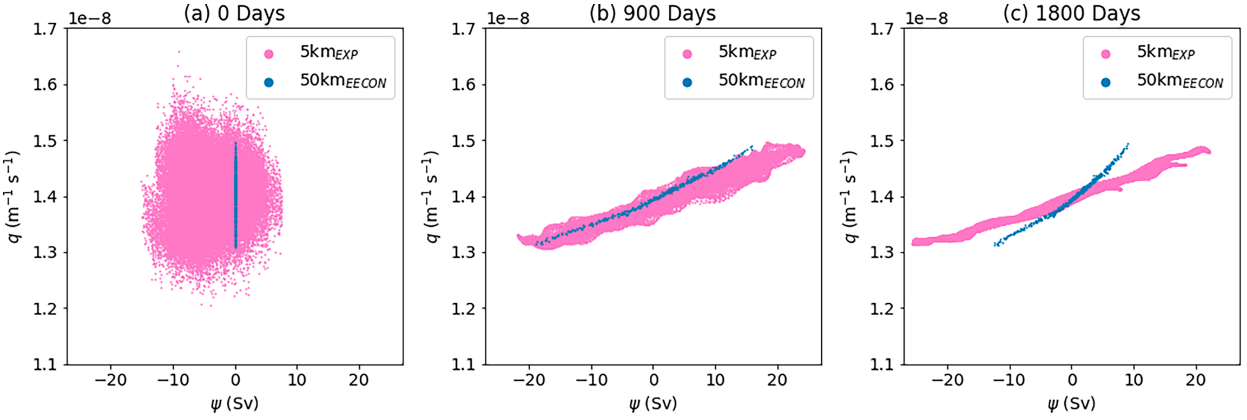

FIG. 7. Scatterplot of streamfunction, ψ, against PV, q, at (a) 0, (b) 900, and (c) 1800 days for $5km_{EXP}$ (pink) and $50km_{EECON}$ (blue) where each point represents a grid point.

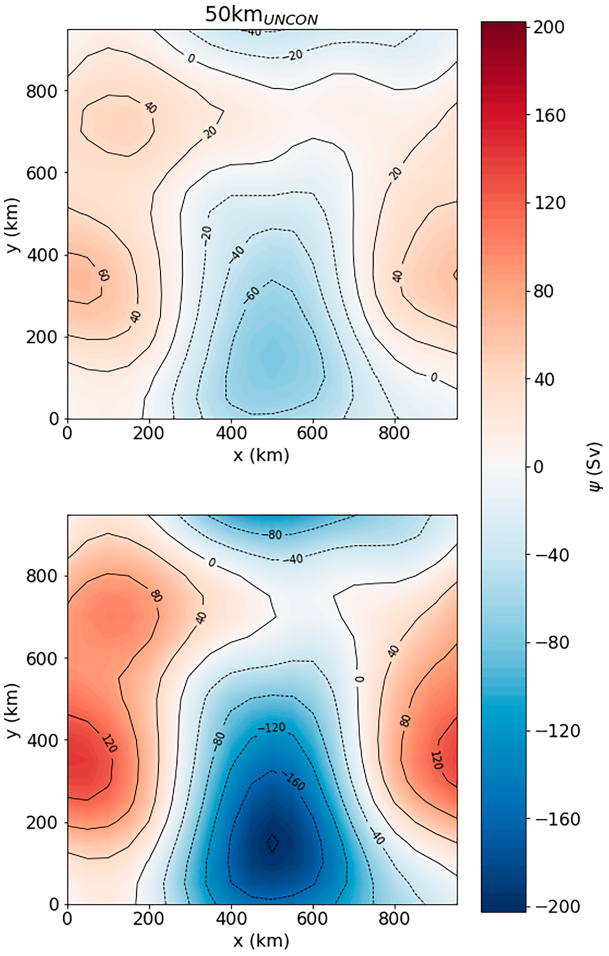

FIG. 8. Time-mean transport streamfunction for $50km_{UNCON}$ over the time periods: (top) 0–1500 days and (bottom) 1501–3000 days.

budget, resulting in a slower depletion of parameterized EKE, K, and a slower growth of MKE. The effect of varying r_Λ on the time scale for growth is exaggerated for smaller values of γ_q, with an increase in r_Λ resulting in an increase in the time scale for growth. Increasing r_Λ decreases Λ, which decreases the magnitude of the eddy PV fluxes, leading to a slower growth rate of MKE as described above, and, correspondingly, a larger time scale for growth. Physically, increasing r_Λ and decreasing γ_q mean that the parameterized eddies persist for a longer period of time. The longer the parameterized eddies are present, the more they mix PV and therefore the more mean-to-eddy potential enstrophy conversion occurs.

6. Discussion

a. Limitations of downgradient PV mixing closures

There are some significant limitations to the parameterization as it is in its current form. First, it is a known problem that, in a multiply connected domain on a β plane employing a downgradient PV mixing closure, integral constraints on the eddy PV fluxes must be satisfied in order for angular momentum conservation to hold (Marshall 1981; Marshall et al. 2012). The current form of the parameterization does not satisfy this constraint. Solutions to this problem have been proposed in previous studies, for example, Eden (2010) introduced a gauge term in the PV closure, which acts as a rotational eddy PV flux and hence does not contribute to the eddy PV flux divergence. Angular momentum is then satisfied through this gauge term. Alternatively, Marshall (1981) and Wardle and Marshall (2000) introduced constraints on κ_{PV} to ensure angular momentum conservation. Further work would be required to implement such a solution into the parameterization, and hence, without this effort, the current form of the parameterization could not be employed successfully in multiply connected domains, e.g., in the circumpolar Southern Ocean.

Additionally, we have specified that the eddy PV fluxes are directed down the mean PV gradient, which is true on average but may not hold locally. For example, upgradient eddy PV fluxes are important in driving time-mean recirculation gyres in western boundary current jets (Waterman et al. 2011). Hence, there are important instances where the parameterization in its current form is not able to capture the full effect of the eddies on the mean flow.

b. Eddy kinetic energy and eddy potential enstrophy budgets

We have made many simplifications in formulating the subgrid-scale budgets employed in this study to inform the parameterization, and it is highly likely that the performance of the parameterization depends on the choices we have made. For example, we have not tested the effect of EKE dissipation in this study since we set $r_K = 0\ s^{-1}$ to mimic the conditions of a weakly dissipative regime. Hence, an understanding of the effect of EKE dissipation on the performance of the parameterization is currently unknown. Mak et al. (2022) showed that when the GEOMETRIC implementation of GM90 is employed, modest variations in the eddy energy dissipation time scale lead to significant changes in the large-scale flow. Thus, it is likely that the representation of EKE dissipation and the value of r_K will affect the large-scale flow produced by the parameterization outlined here. Similarly, the representation of EPEnstr dissipation as linear damping is likely an oversimplification and determining an appropriate value of the EPEnstr dissipation time scale, r_Λ, is not obvious. Testing the parameterization with different iterations of EKE and EPEnstr budgets may be useful in determining the effect and relative importance of each term in the budgets on the large-scale flow.

For simplicity, we have chosen to specify constant values for the parameters associated with the parameterization, but they will likely be variable in both space and time. We have not attempted to define the optimal choice of input parameters, nor have we specified what to optimize toward, since we have tested the parameterization in a highly idealized setup. Understanding of the key controls on the space–time variability of these parameters will be crucial in determining the optimal parameter setup for a more realistic configuration. In particular, investigating the distribution of γ_q and the controls on its value could be of importance.

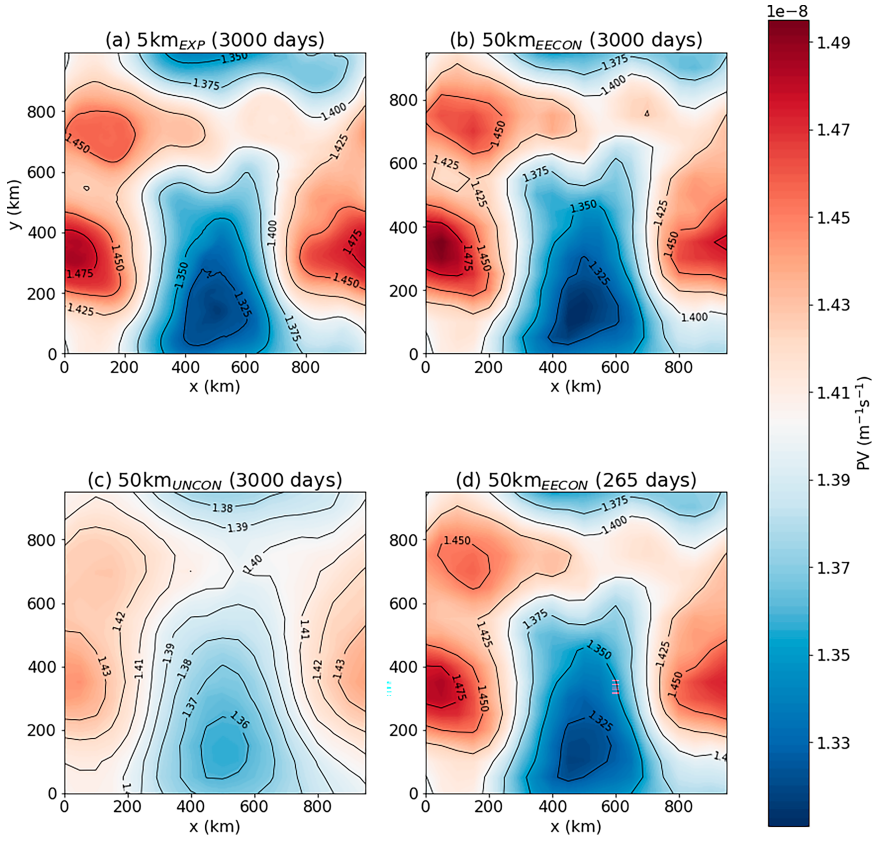

FIG. 9. PV at 3000 days for (a) 5km$_{EXP}$, (b) 50km$_{EECON}$, (c) 50km$_{UNCON}$, and (d) PV for 50km$_{EECON}$ at the time of MPEnstr minimum (265 days) representing the point of maximum PV homogenization.

c. *Implementation in realistic ocean models*

The experiments presented here are highly idealized in order to isolate the effect of the eddies and determine the functionality of the parameterization in a barotropic setup as a first proof of concept. Extending this work to test the parameterization in a realistic ocean setup will require significant work. First, ocean general circulation models (OGCMs) typically solve the momentum equations as opposed to the PV equation, which is solved here. While the eddy PV fluxes do not readily appear in the momentum equation, previous studies have shown that, by taking a suitable averaging operator, one can step forward a transformed version of the primitive equations in which the eddy PV fluxes appear in the momentum equation (e.g., Wardle and Marshall 2000; Young 2012). Such a method would need to be employed to implement this parameterization in a typical OGCM setup.

The introduction of lateral boundaries will affect the large-scale flow produced by the parameterization. Simulations with the same topographical structure but in a closed domain (i.e., with vertical walls on the lateral boundaries with topography intersecting those walls) and free-slip boundary conditions exhibit a reduction in MKE (not shown). Specifically, an eddy-resolving simulation (equivalent to 5km$_{EXP}$ but with lateral walls) has a maximum volume-averaged MKE of 7.5×10^{-5} m^2 s^{-2}, while a coarse-resolution parameterized simulation (equivalent to 50km$_{EECON}$ but with lateral walls) has a maximum volume-averaged MKE of 3.2×10^{-5} m^2 s^{-2}, i.e., 43% of that of the eddy-resolving run.

An important consideration, which will require significant work, is to determine how to integrate the parameterization with a baroclinic eddy parameterization for a continuously stratified fluid. One way forward is to decompose the eddy PV fluxes into baroclinic and barotropic components. Danilov et al. (2019) demonstrated one method of achieving this decomposition in a two-layer quasigeostrophic model; however, determining the appropriate method for the implementation of this parameterization and extending the two-layer method to a continuously stratified fluid requires careful scrutiny. Once decomposed, the baroclinic and barotropic eddy PV fluxes could then be parameterized separately. To maintain energetic consistency, an energetically informed baroclinic eddy parameterization should be employed, for example, a GEOMETRIC implementation of GM90 (Mak et al. 2017, 2018). A unified energy budget should be employed for both the barotropic and baroclinic parameterizations, while an EPEnstr budget is also necessary for the barotropic parameterization. How to unify the energy budget across both barotropic and baroclinic parameterizations remains to be determined. In particular, the

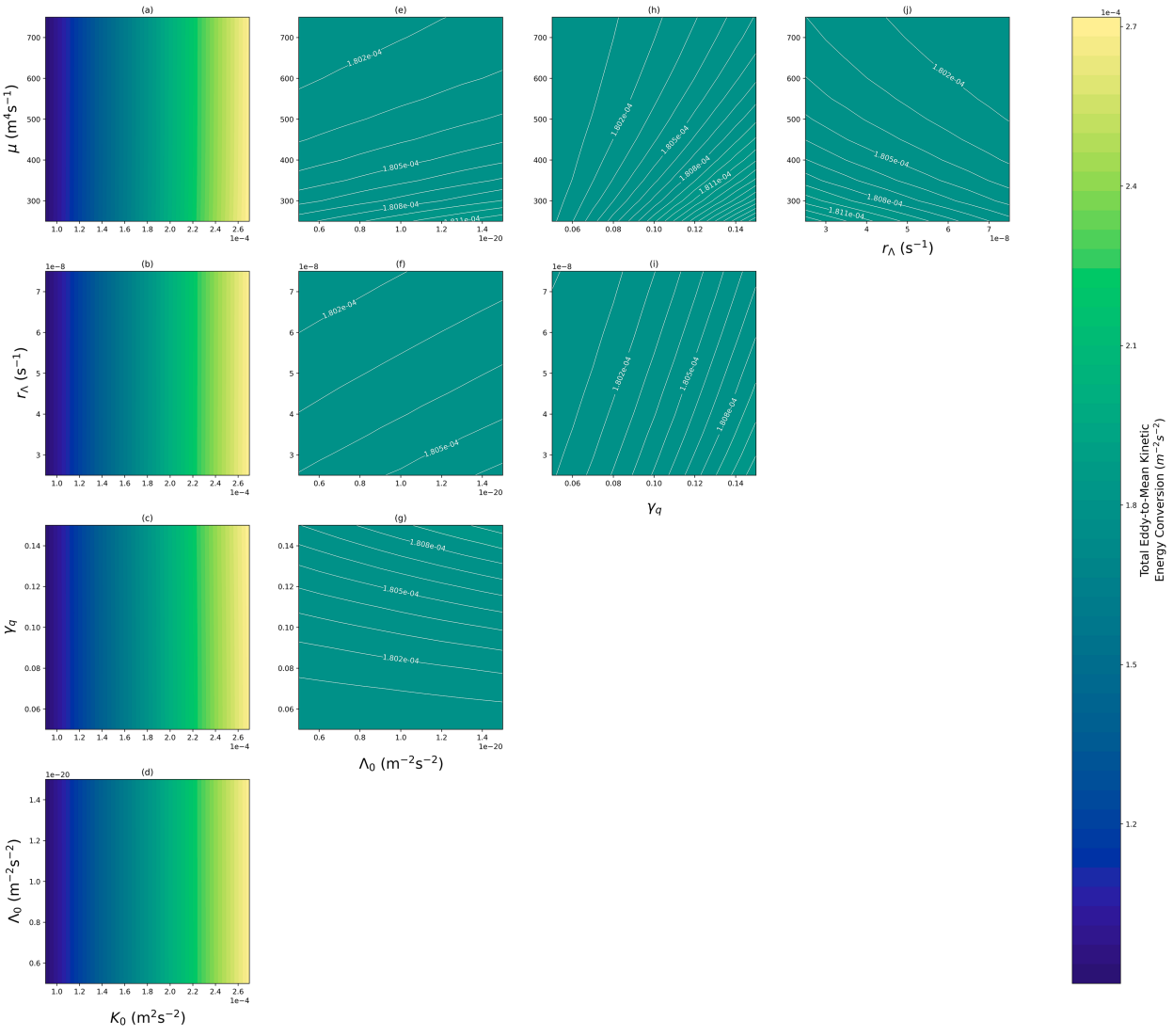

FIG. 10. (a)–(j) Total (time-integrated) volume-averaged eddy-to-mean kinetic energy conversion (contours) for a set of simulations with the same setup as $50km_{EECON}$ in which the input parameters (γ_q, r_Λ, and μ) and the initial conditions (K_0 and Λ_0) are varied by $\pm 50\%$ of their value in $50km_{EECON}$. The variation in values in (e)–(j) is much smaller than the variation in values in (a)–(d), so, for clarity, additional contours are drawn and labeled in (e)–(j).

GEOMETRIC framework leads to a linear dependence on the eddy energy, whereas the method described here produces a nonlinear dependence on both the barotropic EKE and EPEnstr.

7. Summary

We have presented a parameterization for barotropic eddies, which is informed by an EPEnstr budget in addition to an EKE budget. The parameterization imposes downgradient PV mixing in which the strength of the eddy PV fluxes is constrained by both the parameterized EKE and EPEnstr.

The EKE budget employed here includes the following: the bidirectional conversion of kinetic energy between the eddy and mean components of the flow; and a redistribution of EKE, which we represent as advection by the depth-integrated large-scale flow and Laplacian diffusion. The EPEnstr budget includes the mean-to-eddy potential enstrophy conversion, which occurs when the eddies mix PV; a dissipation term, which represents the viscous dissipation of EPEnstr via linear damping; advection by the depth-integrated large-scale flow; and a Laplacian diffusion term. The strength of the parameterized eddy PV fluxes therefore depends on all of these factors. These budgets lead to the following parameters, which must be specified: the EKE dissipation parameter, r_K; the EPEnstr dissipation parameter, r_Λ; and the EKE and EPEnstr diffusion coefficient, μ. Additionally the eddy PV flux efficiency parameter, γ_q, must be specified.

We have tested the parameterization in an idealized, doubly periodic ocean basin with variable bottom topography, simulating freely decaying turbulence on an f plane. Our key findings are as follows:

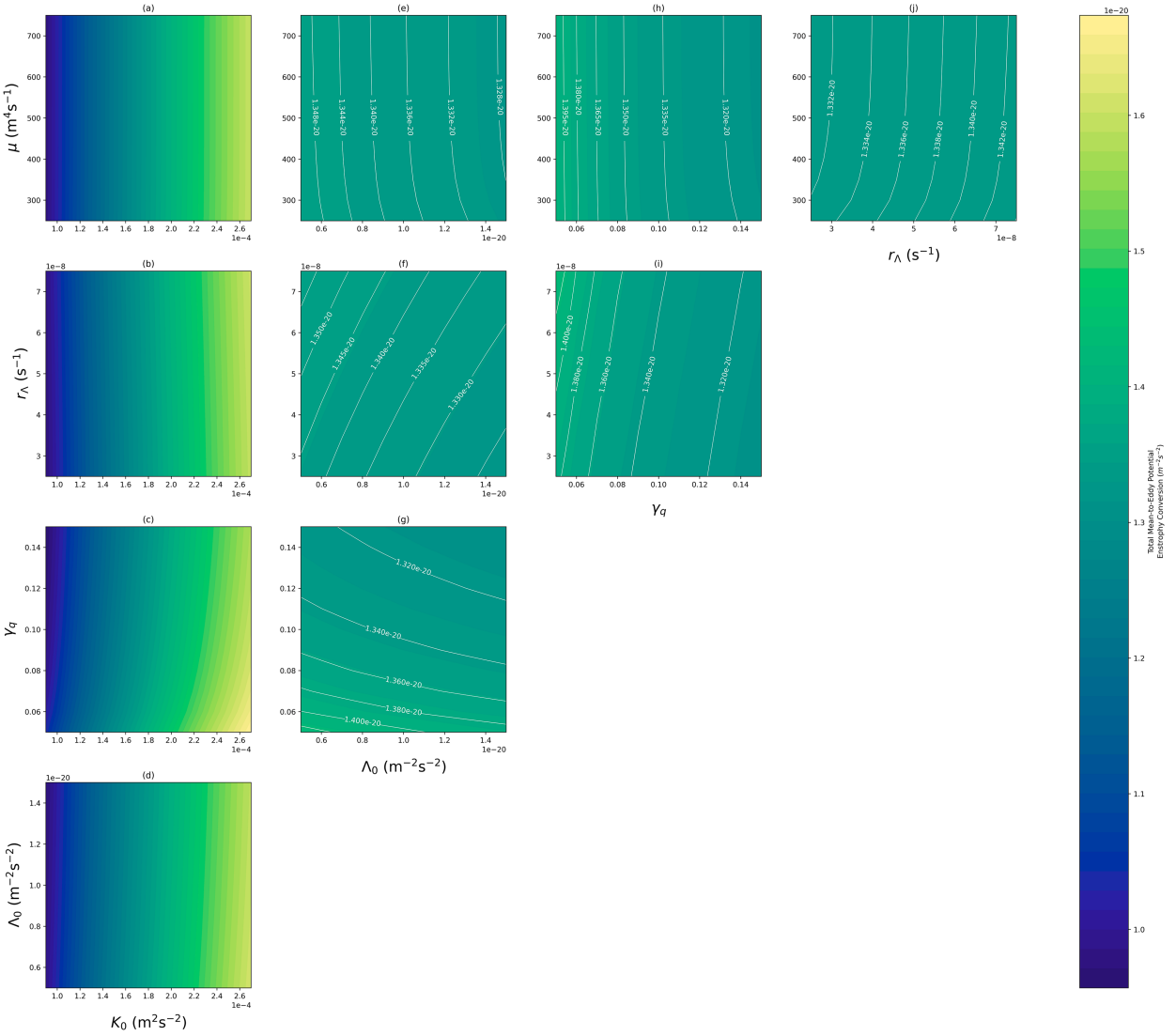

FIG. 11. (a)–(j) Total (time-integrated) volume-averaged mean-to-eddy potential enstrophy conversion (contours) for a set of simulations with the same setup as 50km$_{\text{EECON}}$ where the input parameters (γ_q, r_Λ, and μ) and the initial conditions (K_0 and Λ_0) are varied by ±50% of their value in 50km$_{\text{EECON}}$. The variation in values in (e)–(j) is much smaller than the variation in values in (a)–(d), so for clarity, additional contours are drawn and labeled in (e)–(j).

1) The parameterization leads to a net conversion of kinetic energy from the parameterized eddies to the large-scale flow, resulting in a large-scale topography-following flow.
2) The energetics and enstrophetics of the large-scale flow and parameterized eddy field exhibit similar behavior to that of an eddy-resolving simulation. In particular, both the eddy-to-mean kinetic energy conversion and the mean-to-eddy potential enstrophy conversion increase in magnitude due to the parameterized eddies. This results in an improvement to the large-scale kinetic energy and potential enstrophy when compared to an unconstrained PV mixing parameterization. These findings suggest that the energy and enstrophy constraints imposed in the parameterization are successful in constraining the large-scale flow.
3) The total amount of eddy-to-mean kinetic energy conversion and mean-to-eddy potential enstrophy conversion is predominantly determined by the amount of parameterized EKE in the initial state, K_0. The amount of mean-to-eddy potential enstrophy conversion increases as the time scale for the growth of large-scale kinetic energy increases. This time scale is most sensitive to the changes in the eddy PV flux efficiency parameter, γ_q, and somewhat sensitive to changes in the EPEnstr damping parameter, r_Λ, with a decrease in γ_q or an increase in r_Λ resulting in a longer time scale for growth. The EKE and EPEnstr diffusivity, μ, and the EKE and EPEnstr of the initial state, K_0 and Λ_0, respectively, have a relatively small effect on the time scale for the growth of large-scale kinetic energy.

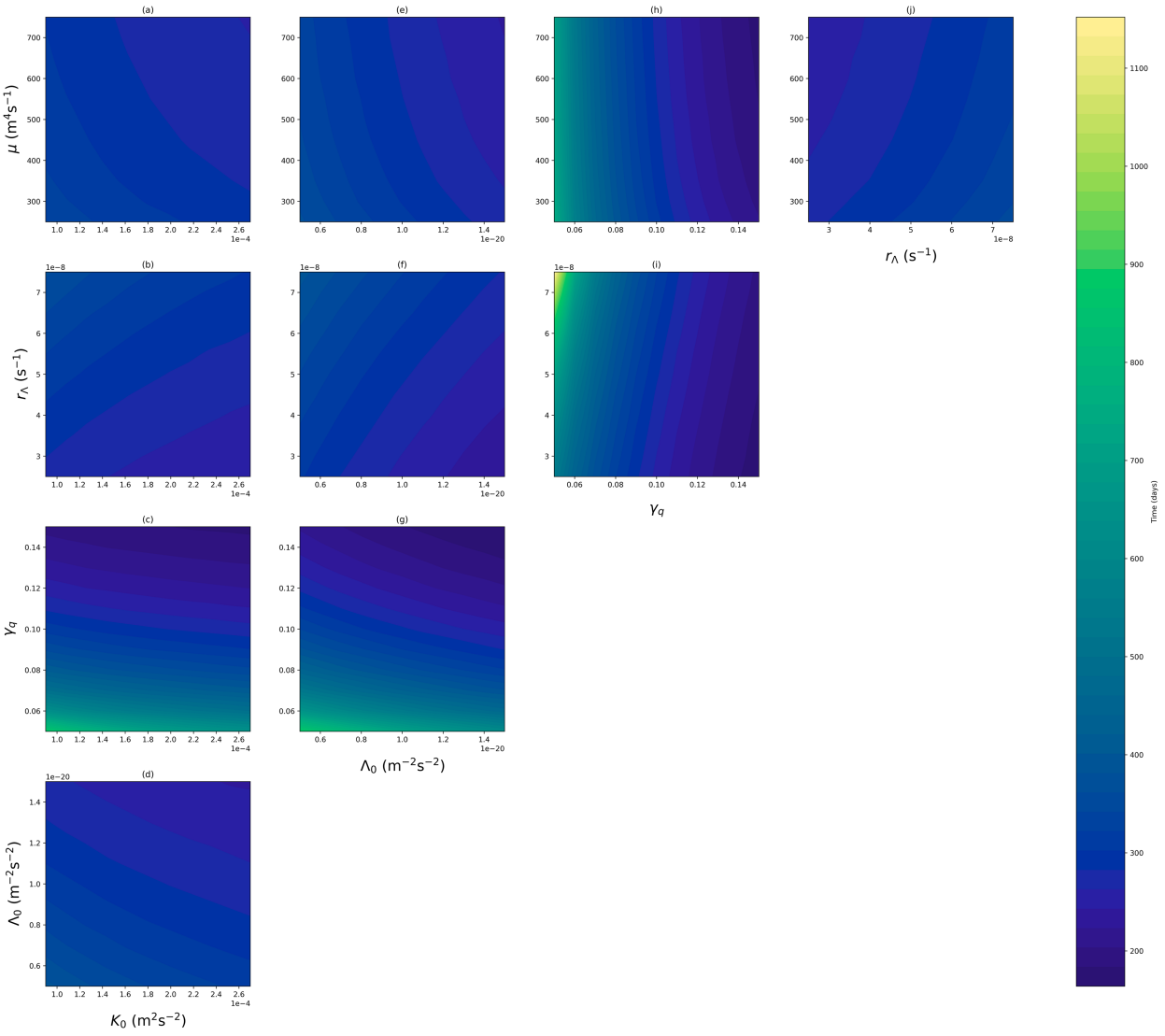

FIG. 12. Time taken for 90% of the initial parameterized EKE, K, to be depleted for a set of simulations with the same setup as $50km_{EECON}$ where the input parameters (γ_q, r_Λ, and μ) and the initial conditions (K_0 and Λ_0) are varied by ±50% of their value in $50km_{EECON}$.

This work adds to the existing literature on eddy parameterizations by proposing a method of constraining the parameterized barotropic eddy PV fluxes by both the EKE and the EPEnstr. This method could constitute a step forward in improving the representation of eddy-seafloor interactions in climate models.

Acknowledgments. Financial support was provided by the U.K. Natural Environment Research Council (NE/S007474/1) and the Oxford-Radcliffe Scholarship. Collaboration was made possible by funding from University College Oxford and the Mitacs Globalink Research Award. SW acknowledges the funding from the Natural Sciences and Engineering Research Council of Canada (NSERC) Discovery Grants Program (NSERC-2020-05799). This work utilized the ARCHER2 U.K. National Supercomputing Service (https://www.archer2.ac.uk/). The authors thank Elizabeth Yankovsky and an anonymous reviewer for insightful comments, which have markedly improved this manuscript.

Data availability statement. The code used for the experiments discussed in this work can be found at https://github.com/rosieeaves/barotropic_model.

REFERENCES

Adcock, S. T., and D. P. Marshall, 2000: Interactions between geostrophic eddies and the mean circulation over large-scale bottom topography. *J. Phys. Oceanogr.*, **30**, 3223–3238, https://doi.org/10.1175/1520-0485(2000)030%3C3223:IBGEAT%3E2.0.CO;2.

Arakawa, A., 1966: Computational design for long-term numerical integration of the equations of fluid motion: Two-dimensional incompressible flow. Part I. *J. Comput. Phys.*, **1**, 119–143, https://doi.org/10.1016/0021-9991(66)90015-5.

Arnold, V. I., 1965: On conditions for non-linear stability of plane stationary curvilinear flows of an ideal fluid. *Dokl. Akad. Nauk SSSR*, **162**, 975–978.

Bachman, S. D., 2019: The GM+E closure: A framework for coupling backscatter with the Gent and McWilliams parameterization. *Ocean Modell.*, **136**, 85–106, https://doi.org/10.1016/j.ocemod.2019.02.006.

Bretherton, F. P., and D. B. Haidvogel, 1976: Two-dimensional turbulence above topography. *J. Fluid Mech.*, **78**, 129–154, https://doi.org/10.1017/S002211207600236X.

Cessi, P., 2008: An energy-constrained parameterization of eddy buoyancy flux. *J. Phys. Oceanogr.*, **38**, 1807–1819, https://doi.org/10.1175/2007JPO3812.1.

Danilov, S., S. Juricke, A. Kutsenko, and M. Oliver, 2019: Toward consistent subgrid momentum closures in ocean models. *Energy Transfers in Atmosphere and Ocean*, Mathematics of Planet Earth, Vol. 1, Springer International Publishing AG, 145–192.

Donohue, K. A., K. L. Tracey, D. R. Watts, M. P. Chidichimo, and T. K. Chereskin, 2016: Mean Antarctic circumpolar current transport measured in Drake Passage. *Geophys. Res. Lett.*, **43**, 11 760–11 767, https://doi.org/10.1002/2016GL070319.

Eden, C., 2010: Parameterising meso-scale eddy momentum fluxes based on potential vorticity mixing and a gauge term. *Ocean Modell.*, **32**, 58–71, https://doi.org/10.1016/j.ocemod.2009.10.008.

——, and R. J. Greatbatch, 2008: Towards a mesoscale eddy closure. *Ocean Modell.*, **20**, 223–239, https://doi.org/10.1016/j.ocemod.2007.09.002.

Eyring, V., S. Bony, G. A. Meehl, C. A. Senior, B. Stevens, R. J. Stouffer, and K. E. Taylor, 2016: Overview of the Coupled Model Intercomparison Project Phase 6 (CMIP6) experimental design and organization. *Geosci. Model Dev.*, **9**, 1937–1958, https://doi.org/10.5194/gmd-9-1937-2016.

Gallet, B., 2024: Two-dimensional turbulence above topography: Condensation transition and selection of minimum enstrophy solutions. *J. Fluid Mech.*, **988**, A13, https://doi.org/10.1017/jfm.2024.365.

Gent, P. R., and J. C. McWilliams, 1990: Isopycnal mixing in ocean circulation models. *J. Phys. Oceanogr.*, **20**, 150–155, https://doi.org/10.1175/1520-0485(1990)020<0150:IMIOCM>2.0.CO;2.

Gregory, J. M., and Coauthors, 2016: The Flux-Anomaly-Forced Model Intercomparison Project (FAFMIP) contribution to CMIP6: Investigation of sea-level and ocean climate change in response to CO_2 forcing. *Geosci. Model Dev.*, **9**, 3993–4017, https://doi.org/10.5194/gmd-9-3993-2016.

Griffies, S. M., and Coauthors, 2009: Coordinated Ocean-Ice Reference Experiments (COREs). *Ocean Modell.*, **26** (1–2), 1–46, https://doi.org/10.1016/j.ocemod.2008.08.007.

——, and Coauthors, 2016: OMIP contribution to CMIP6: Experimental and diagnostic protocol for the physical component of the Ocean Model Intercomparison Project. *Geosci. Model Dev.*, **9**, 3231–3296, https://doi.org/10.5194/gmd-9-3231-2016.

He, J., and Y. Wang, 2024: Multiple states of two-dimensional turbulence above topography. *J. Fluid Mech.*, **994**, R2, https://doi.org/10.1017/jfm.2024.633.

Holland, W. R., and P. B. Rhines, 1980: An example of eddy-induced ocean circulation. *J. Phys. Oceanogr.*, **10**, 1010–1031, https://doi.org/10.1175/1520-0485(1980)010%3C1010:AEOEIO%3E2.0.CO;2.

Holloway, G., 1992: Representing topographic stress for large-scale ocean models. *J. Phys. Oceanogr.*, **22**, 1033–1046, https://doi.org/10.1175/1520-0485(1992)022%3C1033:RTSFLS%3E2.0.CO;2.

Jansen, M. F., and I. M. Held, 2014: Parameterizing subgrid-scale eddy effects using energetically consistent backscatter. *Ocean Modell.*, **80**, 36–48, https://doi.org/10.1016/j.ocemod.2014.06.002.

——, ——, A. Adcroft, and R. Hallberg, 2015: Energy budget-based backscatter in an eddy permitting primitive equation model. *Ocean Modell.*, **94**, 15–26, https://doi.org/10.1016/j.ocemod.2015.07.015.

——, A. Adcroft, S. Khani, and H. Kong, 2019: Toward an energetically consistent, resolution aware parameterization of ocean mesoscale eddies. *J. Adv. Model. Earth Syst.*, **11**, 2844–2860, https://doi.org/10.1029/2019MS001750.

Jones, C. D., and Coauthors, 2016: C4MIP—The Coupled Climate–Carbon Cycle Model Inter-Comparison Project: Experimental protocol for CMIP6. *Geosci. Model Dev.*, **9**, 2853–2880, https://doi.org/10.5194/gmd-9-2853-2016.

Juricke, S., S. Danilov, A. Kutsenko, and M. Oliver, 2019: Ocean kinetic energy backscatter parametrizations on unstructured grids: Impact on mesoscale turbulence in a channel. *Ocean Modell.*, **138**, 51–67, https://doi.org/10.1016/j.ocemod.2019.03.009.

——, ——, N. Koldunov, M. Oliver, and D. Sidorenko, 2020: Ocean kinetic energy backscatter parametrization on unstructured grids: Impact on global eddy-permitting simulations. *J. Adv. Model. Earth Syst.*, **12**, e2019MS001855, https://doi.org/10.1029/2019MS001855.

Mak, J., D. P. Marshall, J. R. Maddison, and S. D. Bachman, 2017: Emergent eddy saturation from an energy constrained eddy parameterisation. *Ocean Modell.*, **112**, 125–138, https://doi.org/10.1016/j.ocemod.2017.02.007.

——, J. R. Maddison, D. P. Marshall, and D. R. Munday, 2018: Implementation of a geometrically informed and energetically constrained mesoscale eddy parameterization in an ocean circulation model. *J. Phys. Oceanogr.*, **48**, 2363–2382, https://doi.org/10.1175/JPO-D-18-0017.1.

——, D. P. Marshall, G. Madec, and J. R. Maddison, 2022: Acute sensitivity of global ocean circulation and heat content to eddy energy dissipation timescale. *Geophys. Res. Lett.*, **49**, e2021GL097259, https://doi.org/10.1029/2021GL097259.

Marshall, D. P., and A. J. Adcroft, 2010: Parameterization of ocean eddies: Potential vorticity mixing, energetics and Arnold's first stability theorem. *Ocean Modell.*, **32**, 188–204, https://doi.org/10.1016/j.ocemod.2010.02.001.

——, J. R. Maddison, and P. S. Berloff, 2012: A framework for parameterizing eddy potential vorticity fluxes. *J. Phys. Oceanogr.*, **42**, 539–557, https://doi.org/10.1175/JPO-D-11-048.1.

Marshall, J. C., 1981: On the parameterization of geostrophic eddies in the ocean. *J. Phys. Oceanogr.*, **11**, 257–271, https://doi.org/10.1175/1520-0485(1981)011%3C0257:OTPOGE%3E2.0.CO;2.

——, and G. Shutts, 1981: A note on rotational and divergent eddy fluxes. *J. Phys. Oceanogr.*, **11**, 1677–1680, https://doi.org/10.1175/1520-0485(1981)011%3C1677:ANORAD%3E2.0.CO;2.

Salmon, R., 1998: *Lectures on Geophysical Fluid Dynamics*. 1st ed., Oxford University Press, 400 pp.

Siegelman, L., and W. R. Young, 2023: Two-dimensional turbulence above topography: Vortices and potential vorticity homogenization. *Proc. Natl. Acad. Sci. USA*, **120**, e2308018120, https://doi.org/10.1073/pnas.2308018120.

Tamarin, T., J. R. Maddison, E. Heifetz, and D. P. Marshall, 2016: A geometric interpretation of eddy Reynolds stresses in barotropic ocean jets. *J. Phys. Oceanogr.*, **46**, 2285–2307, https://doi.org/10.1175/JPO-D-15-0139.1.

Treguier, A. M., I. M. Held, and V. D. Larichev, 1997: Parameterization of quasigeostrophic eddies in primitive equation

Ocean models. *J. Phys. Oceanogr.*, **27**, 567–580, https://doi.org/10.1175/1520-0485(1997)027<0567:POQEIP>2.0.CO;2.

Wardle, R., and J. Marshall, 2000: Representation of eddies in primitive equation models by a PV flux. *J. Phys. Oceanogr.*, **30**, 2481–2503, https://doi.org/10.1175/1520-0485(2000)030<2481:ROEIPE>2.0.CO;2.

Waterman, S., and S. R. Jayne, 2012: Eddy-driven recirculations from a localized transient forcing. *J. Phys. Oceanogr.*, **42**, 430–447, https://doi.org/10.1175/JPO-D-11-060.1.

——, N. G. Hogg, and S. R. Jayne, 2011: Eddy–mean flow interaction in the Kuroshio Extension region. *J. Phys. Oceanogr.*, **41**, 1182–1208, https://doi.org/10.1175/2010JPO4564.1.

Wilson, C., and R. G. Williams, 2004: Why are eddy fluxes of potential vorticity difficult to parameterize? *J. Phys. Oceanogr.*, **34**, 142–155, https://doi.org/10.1175/1520-0485(2004)034<0142:WAEFOP>2.0.CO;2.

Yankovsky, E., S. Bachman, K. S. Smith, and L. Zanna, 2024: Vertical structure and energetic constraints for a backscatter parameterization of ocean mesoscale eddies. *J. Adv. Model. Earth Syst.*, **16**, e2023MS004093, https://doi.org/10.1029/2023MS004093.

Young, R. W., 2012: An exact thickness-weighted average formulation of the Boussinesq equations. *J. Phys. Oceanogr.*, **42**, 692–707, https://doi.org/10.1175/JPO-D-11-0102.1.